A General Model and SINR Analysis of Low Duty-Cycle UWB Access Through Multipath With Narrowband Interference and Rake Reception

Liuqing Yang, *Member, IEEE*, and Georgios B. Giannakis, *Fellow, IEEE*

***Abstract*—Interference from coexisting narrowband services is a critical factor affecting performance of ultra-wideband (UWB) radio communications. There is clearly a need to quantify interference and compare UWB systems on that basis. In this paper, we develop a general Rake reception model along with a unifying transmission framework for low duty-cycle UWB multiple access encompassing existing and novel spreading codes, including direct sequence, digital single- and multi-carrier, time-hopping, and combinations of them. Our unifying framework relies on a digital model, which leads to closed-form performance analysis expressions. Different from existing alternatives that require oversampling, our general model is developed directly from the samples of the Rake receiver output and allows for various Rake finger delay selections. Signal-to-interference-plus-noise ratio analysis and simulations are carried out to assess the relative merits of several UWB systems in the presence of narrowband interference, multipath and additive white Gaussian noise, for both matched-filter and minimum mean square error Rake receivers.**

***Index Terms*—Direct sequence (DS), multi-carrier (MC), multipath, narrowband interference (NBI), Rake, single-carrier (SC), time-hopping (TH), ultra-wideband (UWB).**

I. Introduction

THE growing interest in ultra-wideband (UWB) radios stems from their attractive features that include low-power low-complexity baseband operation, rich multipath diversity, and the potential to enhance user capacity. These features make UWB connectivity suitable for indoor and especially short-range high-rate wireless links in the workplace and at home.

However, coexisting narrowband services introduce interference which degrades performance of UWB radios that rely on spreading schemes to enable multiple access. Widely adopted spreading schemes include time-hopping (TH) and direct sequence (DS) codes [5], [7], [9]. Recently, baseband single-carrier (SC) and multi-carrier (MC) codes have also been introduced to provide improved flexibility in handling multiuser interference (MUI) and narrowband interference (NBI) [12]. In addition, combinations of these codes make it possible to further enhance user capacity, and reinforce low probability of detection [11]. There is clearly a need to compare the performance of these schemes in the presence of NBI and/or dense multipath channels.

Several efforts have been made in this direction. NBI effects to DS-UWB with matched-filter (MF) Rake reception are analyzed in [5] and [7] and NBI in TH-UWB has been studied in the absence of multipath [13]—without accounting for interframe interference (IFI) [1]—and by simulations [6]. Recently, a general discrete-time UWB system model was introduced in [3]. This model subsumes TH and DS transmissions, but requires oversampling of the continuous-time received waveform at subpulse intervals. Consequently, the MF and minimum mean square error (MMSE) receivers developed based on this oversampled discrete-time model call for *oversampled* digital all-Rake configurations. As a result, the performance analysis in [3] neither applies to UWB systems with a limited number of Rake fingers, nor can it accommodate Rake finger delay selections corresponding to low-complexity partial- and selective-Rake receivers that are of practical interest [2].

The main contribution of this paper is a *general* discrete-time model enabling a *unifying* signal-to-interference-plus-noise ratio (SINR) analysis of low duty-cycle UWB multiple access schemes. The generality of the model pertains to: 1) incorporation of transmissions with single- or multi-carrier spreadeing with or without TH (the former introduces challenging IFI effects); 2) propagation through flat or multipath channels in the presence or absence of NBI; and 3) various Rake alternatives with low-complexity frame-rate (or even symbol-rate) receiver sampling per finger. The unifying SINR analysis encompasses DS, SC/MC, and TH spreading codes (or their combinations), and provides a figure of merit for comparing them. Furthermore, it guides the designer to select codes for UWB multiple access by delineating tradeoffs in Rake receiver complexity *versus* resilience to multipath and NBI.

The rest of this paper is organized as follows. The unifying transmission model and the unifying Rake reception model will be introduced in Sections II and III, respectively. In Section IV, the SINR expressions will be derived. Simulations

Manuscript received August 2, 2003; revised February 11, 2004; accepted April 24, 2004. The editor coordinating the review of this paper and approving it for publication is Z. Tian. Prepared through collaborative participation in the Communications and Networks Consortium sponsored by the U.S. Army Research Laboratory under the Collaborative Technology Alliance Program, Cooperative Agreement DAAD19-01-2-0011. The U.S. Government is authorized to reproduce and distribute reprints for Government purposes notwithstanding any copyright notation thereon. This work is also supported by the National Science Foundation under Grant EIA-0324864.

L. Yang is with the Department of Electrical and Computer Engineering, University of Florida, Gainesville, FL 32611 USA (e-mail: lqyang@ece.eufl.edu).

G. B. Giannakis is with the Department of Electrical and Computer Engineering, University of Minnesota, Minneapolis, MN 55455 USA (e-mail: georgios@umn.edu).

Digital Object Identifier 10.1109/TWC.2005.850377

and comparisons will be presented in Section V, and summarizing remarks will be given in Section VI.

Notation: We use bold upper (lower) case letters to denote matrices (column vectors). $\boldsymbol{F}_N$ represents a $N \times N$ fast Fourier transform (FFT) matrix, and $\boldsymbol{I}_N$ stands for a $N \times N$ identity matrix. The $(n+1)$th entry of $\boldsymbol{a}$ is denoted as $[\boldsymbol{a}]_n$, and the $(m+1, n+1)$th entry of $\boldsymbol{A}$ as $[\boldsymbol{A}]_{m,n}$. The symbol $\star$ denotes convolution, $\otimes$ stands for Kronecker product, and $:=$ means 'is defined as.' We use $(\cdot)^{\mathrm{T}}$ and $(\cdot)^{\mathcal{H}}$ for transpose and conjugated transpose, $\lfloor\cdot\rfloor$ and $\lceil\cdot\rceil$ for floor and ceiling operations, $\mathrm{mod}(a,b)$ for modulo operation of a on the basis of b, $\mathrm{rank}\{\boldsymbol{A}\}$ for the rank of matrix $\boldsymbol{A}$, and $\mathrm{diag}\{\boldsymbol{a}\}$ for a diagonal matrix with $\boldsymbol{a}$ on its diagonal.

II. Unifying Transmission Model

Let $s_u(n_s)$ denote the n_sth information-bearing symbol of user u in a UWB system with N_u users. Every symbol is represented by N_f ultrashort pulses $p(t)$ of duration T_p, one per frame of T_f seconds. It follows that the symbol transmitted during the kth frame is given by $s_u(\lfloor k/N_f \rfloor)$ and the resultant symbol duration is thus $T_s := N_f T_f$. With T_p in the order of nanoseconds, the transmission is UWB with bandwidth $B \approx 1/T_p$. Multiple users are separated by user-specific spreading codes, which will be discussed later in detail. We focus on a single user, and treat MUI as noise. Using binary pulse-amplitude modulation (PAM), the uth user's transmitted signal is

$$\nu_u(t) = \sqrt{\frac{\mathcal{E}_u}{N_f}} \sum_{k=0}^{\infty} s_u\left(\left\lfloor \frac{k}{N_f} \right\rfloor\right) c_u(k) p\left[t - kT_f - c_u^{\mathrm{th}}(k) T_c\right] \tag{1}$$

where $\mathcal{E}_u$ is the energy per symbol, and $T_c > T_p$ is the chip duration defined as $T_c := T_f/N_c$ with N_c being the number of chips per frame. Two classes of spreading codes are subsumed by (1): those represented by $c_u(k)$ modify the pulse amplitude from frame to frame; whereas those represented by $c_u^{\mathrm{th}}(k)$ alter the pulse position per frame. The latter are referred to as TH codes. The former, on the other hand, allow for many choices, including the well known DS codes. Later in this section, we will show that $c_u(k)$ can also be designed to yield digital SC- or MC-UWB baseband transmissions [12]. It is worth emphasizing that (1) allows also for combinations of the two classes of spreading codes, e.g., DS–TH codes. Throughout this paper, we will consider "short" spreading codes that are periodic with period N_f. Moreover, $\{c_u(k)\}_{k=0}^{N_f-1}$ will be energy normalized such that $\sum_{k=0}^{N_f-1} c_u^2(k) = N_f$. To put them under a common denominator, we will start with the widely adopted special cases (TH- and DS-UWB), and then briefly review the baseband SC- and MC-UWB spreading codes, which are detailed in [12].

A. TH-UWB and DS-UWB

Choosing $c_u(k) = 1$ and $c_u^{\mathrm{th}}(k) \in [0, N_c - 1]$, $\forall k$ in (1) gives rise to a TH-UWB transmission. Orthogonal TH codes can be chosen such that $c_{u_1}^{\mathrm{th}}(k) \neq c_{u_2}^{\mathrm{th}}(k)$, $\forall u_1 \neq u_2$, $k \in [0, N_f - 1]$. With $c_u^{\mathrm{th}}(k) = 0$, $\forall k$, DS-UWB relies on orthogonal binary sequences $c_u(k) \in \{\pm 1\}$ satisfying: $\sum_{k=0}^{N_f-1} c_{u_1}(k) c_{u_2}(k) = N_f \delta_{u_1 u_2}$. These codes are used in, e.g., [5], [7], and [11].

Notice that with orthogonal DS codes, the maximum number of users N_u equals the number of frames per symbol N_f; whereas with orthogonal TH codes, N_u equals the number of chips per frame N_c. On the other hand, with transmission bandwidth $B \approx 1/T_p$ and bit rate $R = 1/T_s$, the bandwidth expansion factor is given by: $B/R \approx T_s/T_p \approx T_s/T_c = N_f N_c$. Therefore, combined use of orthogonal TH and DS codes can accommodate up to $N_f N_c$ simultaneous users, and thereby exploits the ultra-wide bandwidth more efficiently [11].

B. Baseband Single-Carrier UWB

With $c_u^{\mathrm{th}}(k) = 0$, $\forall k \in [0, N_f - 1]$, digital SC-UWB corresponds to choosing the uth user's spreading code during the kth frame as

$$c_u(k) = \begin{cases} \sqrt{2}\cos(2\pi f_u k) & \forall u \in \left[0, \frac{N_f}{2} - 1\right] \\ \sqrt{2}\sin(2\pi f_u k) & \forall u \in \left[\frac{N_f}{2}, N_f - 1\right] \end{cases} \tag{2}$$

where $f_u := (u + 0.5)/N_f$, $\forall u \in [0, N_f - 1]$ with N_f being even. Different from orthogonal frequency division multiple access (OFDMA) in narrowband systems, the codes in (2) are baseband real, and thus suitable for baseband UWB transmissions without analog carriers. It can be easily verified that these SC spreading codes are also orthogonal: $\sum_{k=0}^{N_f-1} c_{u_1}(k) c_{u_2}(k) = N_f \delta_{u_1 u_2}$.

As in narrowband OFDMA systems, each SC-UWB user spreads every symbol on a single *digital* subcarrier and the resulting transmit-spectrum is distinctly determined by the carrier frequency f_u. This feature shows up clearly in the power spectral density (PSD) of $\nu_u(t)$. The latter turns out to be $\Phi_{vv}(f) = (\mathcal{E}_u/N_f T_s)|P_{s,u}(f)|^2$ for independent and identically distributed (i.i.d.) equiprobable antipodal symbols, where $P_{s,u}(f)$ is the FT of the symbol-level pulse shaper $p_{s,u}(t) := \sum_{k=0}^{N_f-1} c_u(k) p(t - kT_f)$. This FT can be expressed as [12]

$$P_{s,u}(f) = \begin{cases} P(f) \sum_k \mathcal{S}\left(f - \frac{k}{T_f} - \frac{f_u}{T_f}\right) \\ \quad + \mathcal{S}\left(f - \frac{k}{T_f} + \frac{f_u}{T_f}\right), & u \in \left[0, \frac{N_f}{2}\right) \\ -\jmath P(f) \sum_k \mathcal{S}\left(f - \frac{k}{T_f} - \frac{f_u}{T_f}\right) \\ \quad - \mathcal{S}\left(f - \frac{k}{T_f} + \frac{f_u}{T_f}\right), & u \in \left[\frac{N_f}{2}, N_f\right) \end{cases} \tag{3}$$

where $P(f) := \mathcal{F}\{p(t)\}$, and $\mathcal{S}(f) := (N_f/\sqrt{2}) \exp[-\jmath\pi(N_f - 1)T_f f] \mathrm{sinc}(T_s f)$ with $\mathrm{sinc}(f) := \sin(\pi f)/(\pi f)$. Fig. 1 depicts the transmit-PSD, confirming that every digital "carrier" corresponds to distinct frequency bands, i.e., sinc main lobes, each of width $2/T_s$ Hz. Evidently, individual digital carrier bands can suffer from cochannel NBI at various degrees; and those that are heavily affected can be avoided. Also clear from Fig. 1 is that different from narrowband OFDMA, where each user occupies a single frequency band, each SC-UWB user occupies $2T_f/T_p$

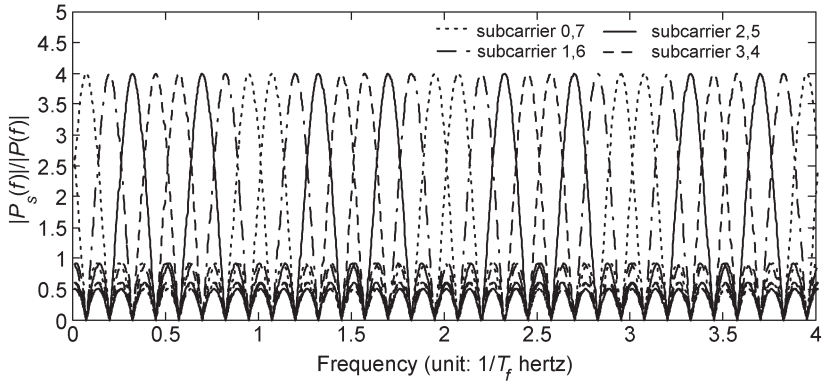

Fig. 1. Subcarriers in baseband SC-UWB ($N_f = 8, T_f = 4T_p$).

frequency bands. This enables SC-UWB to enjoy full multipath diversity gains [12].

C. Baseband Multi-Carrier UWB

Each user here utilizes all $N_u = N_f$ digital subcarriers $\{\boldsymbol{g}_k\}_{k=0}^{N_f-1}$

$$[\boldsymbol{g}_k]_n = \begin{cases} \sqrt{\frac{1}{N_f}}\cos\left(\frac{2\pi n}{N_f}k\right), & n = 0, \text{ or, } n = \frac{N_f}{2} \\ \sqrt{\frac{2}{N_f}}\cos\left(\frac{2\pi n}{N_f}k\right), & n \in \left[1, \frac{N_f}{2} - 1\right] \\ \sqrt{\frac{2}{N_f}}\sin\left(\frac{2\pi n}{N_f}k\right), & n \in \left[\frac{N_f}{2} + 1, N_f - 1\right] \end{cases}. \tag{4}$$

With $\{\boldsymbol{c}_u^{(o)}\}_{u=0}^{N_f-1}$ denoting any set of orthogonal spreading codes of length N_f, the spreading codes for MC-UWB access are

$$c_u(k) = \boldsymbol{g}_k^{\mathrm{T}}\boldsymbol{c}_u^{(o)} \quad \forall k, u \in [0, N_f - 1]. \tag{5}$$

These codes are clearly orthogonal so long as $\{\boldsymbol{c}_u^{(o)}\}_{u=0}^{N_f-1}$ are orthogonal. For a detailed description of MC-UWB, the reader is referred to [12]. Much as with SC-UWB, each MC-UWB carrier occupies several distinct frequency bands, in a form similar to (3), and allows for flexible NBI avoidance. But different from SC-UWB, each MC-UWB user utilizes all digital carriers. This will turn out to imply that with appropriate selection of $\{\boldsymbol{c}_u^{(o)}\}_{u=0}^{N_f-1}$, MC-UWB enjoys bit error rate (BER) performance that is independent of $c_u(k)$, in the presence of NBI. We will revisit this important issue in the ensuing sections.

Similar to DS, each SC or MC spreading code can also be paired with a TH code to yield SC–TH- or MC–TH-UWB transmission.

So far, we have seen that the unifying transmission model (1) not only subsumes TH-, DS-, SC-, and MC-UWB, but also combinations of them. The latter can be implemented through multistage spreading operations as detailed in [11].

III. General Rake Reception Model

In order to facilitate performance analysis and comparison, we will next establish a general Rake reception model, starting with the signal received after multipath propagation. Let $h(t) := \sum_{l=0}^{L}\alpha_l\delta(t - \tau_l)$ denote the multipath channel with $L + 1$ paths. The continuous-time received waveform is then given by [cf. (1)]

$$\begin{aligned} r_u(t) &= \nu_u(t) \star h(t) + w(t) + j(t) \\ &= \sqrt{\frac{\mathcal{E}_u}{N_f}}\sum_{k=0}^{\infty} s_u\left(\left\lfloor\frac{k}{N_f}\right\rfloor\right) c_u(k) g\left[t - kT_f - c_u^{\mathrm{th}}(k)T_c\right] \\ &\quad + w(t) + j(t) \end{aligned} \tag{6}$$

where $g(t) := p(t) \star h(t) = \sum_{l=0}^{L}\alpha_l p(t - \tau_l)$ is the composite pulse-multipath channel with delay spread $\tau_L + T_p$, $w(t)$ is the additive white Gaussian noise (AWGN) and $j(t)$ denotes NBI. Since the frame duration T_f is up to our disposal, we choose $T_f > \tau_L + T_p$ to avoid IFI and intersymbol interference (ISI), in the absence of TH. This assumption simplifies our analysis considerably, but confines our scope to *low duty-cycle* UWB systems. Relaxing this assumption is of interest, because it allows for higher rate transmissions, but goes beyond the scope of this paper.

To collect multipath diversity, Rake reception is often adopted in UWB systems [10]. Rake receivers with N fingers weigh and sum outputs from a bank of N correlators (diversity combining). During the kth frame of each symbol, the template for the nth correlator (Rake finger with delay $\tilde{\tau}_n$)[1] is the pulse $p(t)$ delayed by $kT_f + c_u^{\mathrm{th}}(k)T_c + \tilde{\tau}_n$. For fingers to capture *resolvable* multipath returns, their delay must satisfy $\tilde{\tau}_n - \tilde{\tau}_{n-1} \geq T_p$, which implies that at most $\bar{N} := \lfloor\tau_L/T_p\rfloor$ fingers would suffice to collect the available multipath diversity. In practice, $N \leq \bar{N}$ (all-Rake, partial-Rake, or selective-Rake) is often chosen to tradeoff error performance with complexity [2].

In the following, we will first consider DS-, SC-, or MC-UWB reception in the absence of TH, and then generalize our model when TH is also present.

A. DS/SC/MC-UWB Without TH

In this case, $c_u^{\mathrm{th}}(k) = 0$, $\forall m$, implies that the template for the nth finger's correlator is given by: $p(t - kT_f - \tilde{\tau}_n)$, during

[1]Our usage of tilde for Rake finger delays ($\tilde{\tau}_n$) is to stress that those do not have to necessarily coincide with the multipath channel delays (τ_n).

the kth frame. Accordingly, the nth finger's correlator output during the kth frame is:

$$x_u(k;n) = \int_{kT_f+\tilde{\tau}_n}^{kT_f+\tilde{\tau}_n+T_p} r_u(t)p(t-kT_f-\tilde{\tau}_n)\mathrm{d}t. \quad (7)$$

To establish the input–output (I/O) relationship in digital form, let us define $\tilde{\alpha}_n := \int_{\tilde{\tau}_n}^{\tilde{\tau}_n+T_p} g(t)p(t-\tilde{\tau}_n)\mathrm{d}t$ to represent the "effective channel amplitude" at the nth finger's correlator output. Using our low duty-cycle assumption $T_f > \tau_L + T_p$, it then follows that $\int_{kT_f+\tilde{\tau}_n}^{kT_f+\tilde{\tau}_n+T_p} g(t-mT_f)p(t-kT_f-\tilde{\tau}_n)\mathrm{d}t = \tilde{\alpha}_n\delta_{\mathrm{km}}$. Taking this into account when substituting (6) to (7), we obtain: $x_u(k;n) = (\mathcal{E}_u/N_f)^{1/2}s_u(\lfloor k/N_f \rfloor)c_u(k)\tilde{\alpha}_n + w(k;n) + j(k;n)$, where $w(k;n)$ and $j(k;n)$ denote respectively the sampled additive noise and NBI at the correlator output of the nth finger, during the kth frame. Notice that the filtered and sampled AWGN $w(k;n)$ stays white, since the $\tilde{\tau}_n$'s are spaced sufficiently apart.

Stacking the correlator output samples from all N fingers during the kth frame, we form

$$\begin{aligned}\boldsymbol{x}_u(k) &:= [\, x_u(k;0) \quad x_u(k;1) \quad \ldots \quad x_u(k;N-1)\,]^{\mathrm{T}} \\ &= \sqrt{\frac{\mathcal{E}_u}{N_f}}s_u\left(\left\lfloor \frac{k}{N_f} \right\rfloor\right)c_u(k)\tilde{\boldsymbol{\alpha}} + \boldsymbol{w}(k) + \boldsymbol{j}(k) \quad (8)\end{aligned}$$

where $\tilde{\boldsymbol{\alpha}}$, $\boldsymbol{w}(k)$, and $\boldsymbol{j}(k)$ are all $N \times 1$ vectors constructed by stacking $\tilde{\alpha}_n$, $w(k;n)$, and $j(k;n)$ for $n \in [0, N-1]$. Recalling that each symbol is conveyed by N_f pulses, we need to collect a total of NN_f correlator output samples, N per frame, in order to decode one symbol. To this end, we concatenate vectors $\{\boldsymbol{x}_u(k)\}_{k=n_sN_f}^{(n_s+1)N_f-1}$ into a super vector of size $N_fN \times 1$ as [cf. (8)]

$$\begin{aligned}\boldsymbol{y}_u(n_s) &:= [\, \boldsymbol{x}_u^{\mathrm{T}}(n_sN_f) \quad \ldots \quad \boldsymbol{x}_u^{\mathrm{T}}(n_sN_f+N_f-1)\,]^{\mathrm{T}} \\ &= \sqrt{\frac{\mathcal{E}_u}{N_f}}s_u(n_s)(\boldsymbol{c}_u \otimes \tilde{\boldsymbol{\alpha}}) + \boldsymbol{\eta}(n_s) \quad (9)\end{aligned}$$

where $\boldsymbol{c}_u := [c_u(0), \ldots, c_u(N_f-1)]^{\mathrm{T}}$ is the spreading code vector and $\boldsymbol{\eta}(n_s) := [\boldsymbol{w}^{\mathrm{T}}(n_sN_f) + \boldsymbol{j}^{\mathrm{T}}(n_sN_f), \ldots, \boldsymbol{w}^{\mathrm{T}}(n_sN_f + N_f - 1) + \boldsymbol{j}^{\mathrm{T}}(n_sN_f + N_f - 1)]^{\mathrm{T}}$ is the $N_fN \times 1$ noise vector that consists of AWGN, MUI, and NBI present over the n_sth symbol duration.

Notice that $\boldsymbol{y}_u(n_s)$ contains nothing but the correlator outputs collected from N fingers over N_f consecutive frames corresponding to the n_sth symbol. Relative to [3], which requires subpulse-rate oversampling, (9) is formed by frame-rate samples per Rake finger. To decode a symbol, diversity combining needs to be carried out. With the $N_fN \times 1$ weight vector $\boldsymbol{\beta}$, diversity combining yields the following decision statistic for the n_sth symbol: $z_u(n_s) := \boldsymbol{\beta}^{\mathrm{T}}\boldsymbol{y}_u(n_s)$.

In the *absence* of NBI, maximum ratio combining (MRC) is optimal since $\boldsymbol{\eta}$ in (9) becomes white Gaussian. MRC then corresponds to MF weights $\boldsymbol{\beta}_{\mathrm{mf}} := \boldsymbol{c}_u \otimes \tilde{\boldsymbol{\alpha}}$. But in the *presence* of NBI, the color of $\boldsymbol{\eta}(n_s)$ renders MF reception suboptimal and motivates the usage of MMSE weights, which for our sampled vector model in (9) are

$$\begin{aligned}\boldsymbol{\beta}_{\mathrm{mmse}} &:= \frac{\mathcal{E}_u}{N_f}\left[\boldsymbol{R}_\eta + \frac{\mathcal{E}_u}{N_f}(\boldsymbol{c}_u \otimes \tilde{\boldsymbol{\alpha}})(\boldsymbol{c}_u \otimes \tilde{\boldsymbol{\alpha}})^{\mathrm{T}}\right]^{-1}(\boldsymbol{c}_u \otimes \tilde{\boldsymbol{\alpha}}) \\ &= \frac{\mathcal{E}_u}{N_f}\boldsymbol{R}_\eta^{-1}(\boldsymbol{c}_u \otimes \tilde{\boldsymbol{\alpha}}) \\ &\quad \times \left[1 + \frac{\mathcal{E}_u}{N_f}(\boldsymbol{c}_u \otimes \tilde{\boldsymbol{\alpha}})^{\mathrm{T}}\boldsymbol{R}_\eta^{-1}(\boldsymbol{c}_u \otimes \tilde{\boldsymbol{\alpha}})\right]^{-1} \quad (10)\end{aligned}$$

where $\boldsymbol{R}_\eta := E\{\boldsymbol{\eta}(n_s)\boldsymbol{\eta}^{\mathrm{T}}(n_s)\}$. As usual, if $\boldsymbol{\eta}$ is white, $\boldsymbol{\beta}_{\mathrm{mmse}}$ boils down to $\boldsymbol{\beta}_{\mathrm{mf}}$.

In order to quantify error performance of MF and MMSE Rake receivers, one needs to know the structure of $\boldsymbol{R}_\eta$. It is well known that uniformly sampling a wide sense stationary (WSS) process yields a WSS sequence. But in order to encompass various selections of Rake fingers, we generally allow the delays $\{kT_f + \tilde{\tau}_n\}$ to be nonuniformly spaced across k and n; i.e., even though for a given n, delays $kT_f + \tilde{\tau}_n$ are uniform across frames (k), for a given k, $\tilde{\tau}_n$'s are often nonuniformly spaced within a frame, as for example in selective-Rake receivers. Consequently, the entries of $\boldsymbol{\eta}(n_s)$ are nonuniformly sampled noise variables. With N Rake fingers per frame, nonuniformly sampled noise per frame turns out to be cyclostationary with period N. As a result, $\boldsymbol{R}_\eta$ has a block-Toeplitz structure, but each $N \times N$ block of $\boldsymbol{R}_\eta$ is not necessarily Toeplitz. It is useful to specify the form of $\boldsymbol{R}_\eta$ for various Rake finger selections. The latter will be represented with a finger selection matrix $\boldsymbol{S}$, whose construction is detailed next.

Let T_f/T_p be an integer N_p without loss of generality. With Rake finger delays being integer multiples of T_p, N_p is an upper bound on the number of Rake fingers N; that is, $N \leq \bar{N} < N_p$ and the N Rake fingers can be thought of as being *selected* from a total of N_p possible ones. This selection can be represented with a delay selection matrix $\boldsymbol{S}$. Let us sort the N (generally non equi-spaced) finger delays in an increasing order and let $\tilde{\tau}_n = i_n \cdot T_p$, with integers $\{i_n\}_{n=0}^{N-1} \in [0, \bar{N}-1]$. Using these i_n's, the $N_p \times N$ delay selection matrix $\boldsymbol{S}$ is constructed so that the nth column of $\boldsymbol{S}$ is $\boldsymbol{e}_{i_n+1}$; i.e., the (i_n+1)th column of $\boldsymbol{I}_{N_p}$. Let us take as an example the partial-Rake reception, where the first $N < \bar{N}$ delays are chosen; i.e., $\tilde{\tau}_n = n \cdot T_p$, $\forall n \in [0, N-1]$. In this case, the delay selection matrix is given by $\boldsymbol{S} = [\boldsymbol{I}_N \ \boldsymbol{0}_{N\times(N_p-N)}]^{\mathrm{T}}$. Since the latter pads $(N_p - N)$ zeros to an $N \times 1$ vector, we term it a zero-padding matrix and denote it from now on as $\boldsymbol{T}_{N_p,N}$.

Corresponding to the N_p possible uniformly spaced Rake finger delays in a given frame, there are N_p uniform noise samples. Collecting these noise samples over N_f frames into an $N_fN_p \times 1$ vector $\bar{\boldsymbol{\eta}}(n_s)$ leads to a correlation matrix $\boldsymbol{R}_{\bar{\eta}} := E\{\bar{\boldsymbol{\eta}}(n_s)\bar{\boldsymbol{\eta}}^{\mathrm{T}}(n_s)\}$ that is Toeplitz, simply because the entries of $\bar{\boldsymbol{\eta}}(n_s)$ are uniformly sampled noise variables. As $\boldsymbol{S}$ selects the Rake finger delays, it also selects from $\bar{\boldsymbol{\eta}}(n_s)$ the noise samples corresponding to the selected delays. With such a selection process being repeated in each frame comprising a symbol, we have $\boldsymbol{\eta} = (\boldsymbol{I}_{N_f} \otimes \boldsymbol{S}^{\mathrm{T}})\bar{\boldsymbol{\eta}}(n_s)$. As a result, its correlation matrix $\boldsymbol{R}_\eta = (\boldsymbol{I}_{N_f} \otimes \boldsymbol{S}^{\mathrm{T}})\boldsymbol{R}_{\bar{\eta}}(\boldsymbol{I}_{N_f} \otimes \boldsymbol{S})$ is an $N_fN \times N_fN$ block-Toeplitz matrix with submatrices of size $N \times N$.

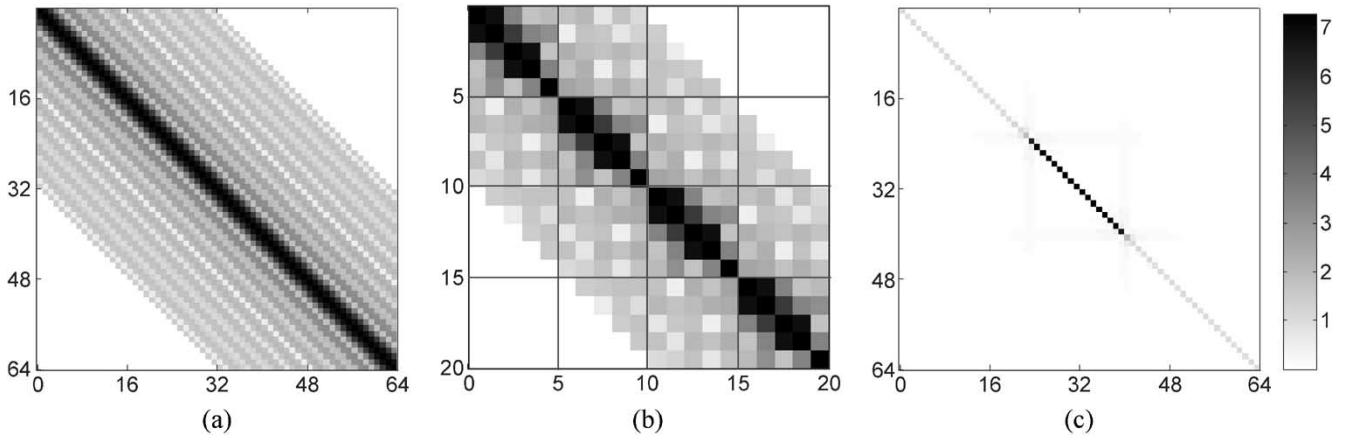

Fig. 2. (a) Structure of $\boldsymbol{R}_{\bar{\eta}}$; (b) structure of $\boldsymbol{R}_{\eta}$; and (c) structure of $\boldsymbol{\Phi}$. $N_f = 4$, $N_p = 16$, $N = 5$.

An example of $\boldsymbol{R}_{\bar{\eta}}$ is illustrated in Fig. 2(a), with $N_f = 4$ and $N_p = 16$. Its Toeplitz structure is evident. With the same parameters, Fig. 2(b) illustrates an example of $\boldsymbol{R}_{\eta}$, using the selection matrix $\boldsymbol{S} = [\,\boldsymbol{e}_7 \quad \boldsymbol{e}_8 \quad \boldsymbol{e}_{10} \quad \boldsymbol{e}_{11} \quad \boldsymbol{e}_{14}\,]$ with $N = 5$ and i_n's being 6, 7, 9, 10, and 13. Evidently, $\boldsymbol{R}_{\eta}$ is not Toeplitz, but rather block-Toeplitz with identical submatrices sitting along any diagonal with direction from northwest to southeast. Also notice that due to the choice of $\boldsymbol{S}$, these 5×5 submatrices are not Toeplitz. They will become Toeplitz if and only if Rake finger delays are equi-spaced.

B. DS/SC/MC-UWB With TH

When TH spreading codes are also employed, deriving an I/O model like (9) is more challenging. The template for the nth correlator is now $p(t)$ delayed by $kT_f + c_u^{\rm th}(k)T_c + \tilde{\tau}_n$, during the kth frame. If the Rake samples corresponding to the $(k+1)$th pulse do not involve the kth pulse and the Rake samples corresponding to the kth pulse do not involve the $(k+1)$th pulse, then the correlator output samples will not experience IFI. Such a situation translates to the following conditions $\forall k \in [0, N_f - 2]$

$$\begin{aligned} T_f + c_u^{\rm th}(k+1)T_c + \tilde{\tau}_0 &\geq c_u^{\rm th}(k)T_c + \tau_L + T_p \\ T_f + c_u^{\rm th}(k+1)T_c &\geq c_u^{\rm th}(k)T_c + \tilde{\tau}_{N-1} + T_p. \end{aligned} \quad (11)$$

Conditions (11) are not guaranteed in general. This necessitates generalizing our Rake reception model (9) to include the IFI induced by TH.

Without loss of generality, we let $T_c = T_p$. Indeed, for any TH code $c_u^{\rm th}(k; T_c)$ with chip duration $T_c = K_{cp}T_p$ (with integer $K_{cp} > 1$), one can always construct an equivalent TH code with chip duration T_p as: $c_u^{\rm th}(k; T_p) = K_{cp}c_u^{\rm th}(k; K_{cp}T_p)$. Therefore, it suffices to consider the $T_c = T_p$ case only.

Let us start with the TH-only case by setting $c_u(k) = 1$, $\forall k$. To establish the I/O relationship, let the $N_p \times 1$ vector $\bar{\boldsymbol{\alpha}}$ contain the N_p possible output samples per frame, one sample per T_p. From the definition of the delay selection matrix $\boldsymbol{S}$, it follows that $\tilde{\boldsymbol{\alpha}} = \boldsymbol{S}^{\rm T}\bar{\boldsymbol{\alpha}}$. Consequently, the vector $\bar{\boldsymbol{y}}_u(n_s)$, which consists of all possible $N_f N_p$ outputs during the n_sth symbol duration, can be expressed as

$$\begin{aligned} \bar{\boldsymbol{y}}_u(n_s) = \sqrt{\frac{\mathcal{E}_u}{N_f}} s_u(n_s) \left(\begin{bmatrix} \boldsymbol{A}_0 \\ \boldsymbol{A}_1 \\ \vdots \\ \boldsymbol{A}_{N_f-1} \end{bmatrix} + \begin{bmatrix} \boldsymbol{0}_{N_p \times N_p} \\ \boldsymbol{B}_0 \\ \vdots \\ \boldsymbol{B}_{N_f-2} \end{bmatrix} \right) \bar{\boldsymbol{\alpha}} \\ + \sqrt{\frac{\mathcal{E}_u}{N_f}} s_u(n_s - 1) \begin{bmatrix} \boldsymbol{B}_{N_f-1} \\ \boldsymbol{0}_{N_p \times N_p} \\ \vdots \\ \boldsymbol{0}_{N_p \times N_p} \end{bmatrix} \bar{\boldsymbol{\alpha}} + \bar{\boldsymbol{\eta}}(n_s) \end{aligned} \quad (12)$$

where $\boldsymbol{A}_k := (\boldsymbol{J}_{N_p})^{c_u^{\rm th}(k)}$, and $\boldsymbol{B}_k := (\boldsymbol{J}_{N_p}^{\rm T})^{\bar{c}_u^{\rm th}(k)}$ with $\boldsymbol{J}_{N_p}$ being a $N_p \times N_p$ lower triangular Toeplitz matrix with first column $[\,0 \quad 1 \quad 0 \quad \ldots \quad 0\,]^{\rm T}$, $\bar{c}_u^{\rm th}(k) := N_p - c_u^{\rm th}(k)$, $\forall k$, and $\bar{\boldsymbol{\eta}}(n_s)$ is the $N_f N_p \times 1$ NBI-bearing noise vector that we detailed in the previous section. Notice that both IFI and ISI are present in (12): the $s_u(n_s - 1)$ dependent term represents ISI; while the second term in parentheses relates adjacent frames and incorporates IFI. Since $(\boldsymbol{J}_{N_p}^{\rm T})^{N_p} = \boldsymbol{0}_{N_p \times N_p}$, IFI vanishes if $c_u^{\rm th}(k) = 0$, $\forall k \in [0, N_f - 2]$, and ISI vanishes if $c_u^{\rm th}(N_f - 1) = 0$. In the following, we will null the last frame of the TH code per symbol; i.e., set $c_u^{\rm th}(N_f - 1) = 0$ and impose no constraints on the rest. With this guard frame, ISI is eliminated and (12) becomes:

$$\bar{\boldsymbol{y}}_u = \sqrt{\frac{\mathcal{E}_u}{N_f}} s_u(\boldsymbol{\Theta} + \boldsymbol{\Psi}) \left(\boldsymbol{1}_{N_f \times 1} \otimes \bar{\boldsymbol{\alpha}} \right) + \bar{\boldsymbol{\eta}} \quad (13)$$

where the symbol index n_s is omitted for notational brevity, $\boldsymbol{\Theta} := \mathrm{diag}\{\boldsymbol{A}_0, \ldots, \boldsymbol{A}_{N_f-1}\}$ and $\boldsymbol{\Psi} := \mathrm{diag}\{\boldsymbol{0}_{N_p \times N_p}, \boldsymbol{B}_0, \ldots, \boldsymbol{B}_{N_f-2}\}(\boldsymbol{J}_{N_f} \otimes \boldsymbol{I}_{N_p})$ are both $N_f N_p \times N_f N_p$ square matrices. Generalization of (13) to also include DS/SC/MC spreading codes is then straightforward

$$\bar{\boldsymbol{y}}_u = \sqrt{\frac{\mathcal{E}_u}{N_f}} s_u(\boldsymbol{\Theta} + \boldsymbol{\Psi})(\boldsymbol{c}_u \otimes \bar{\boldsymbol{\alpha}}) + \bar{\boldsymbol{\eta}}. \quad (14)$$

It is easy to verify that $\bar{\boldsymbol{y}}_u$ in (14) has $N_f N_p$ entries and contains all-Rake finger outputs by construction. But the structures of $\boldsymbol{\Theta}$ and $\boldsymbol{\Psi}$ imply that $\bar{\boldsymbol{y}}_u$ may contain noise-only entries. Moreover,

since $\bar{\boldsymbol{\alpha}}$ contains entries that may not be selected by $\boldsymbol{S}$, $\bar{\boldsymbol{y}}_u$ may also contain entries that do *not* appear as Rake outputs. This should be expected since N_f pulses can yield at most $N_fN < N_fN_p$ nonzero correlator outputs with an N-finger Rake, even in the absence of IFI. Therefore, before Rake combining, we need to "squeeze out" these "excess entries" of $\bar{\boldsymbol{y}}_u$. In the absence of TH, it turns out that these excess entries can be removed using the selection matrix $\boldsymbol{S}$ as follows:

Lemma 1: For any arbitrary selection of Rake delays described by matrix $\boldsymbol{S}$, if the TH code is absent, then $\boldsymbol{y}_u = (\boldsymbol{I}_{N_f} \otimes \boldsymbol{S})^{\mathrm{T}} \bar{\boldsymbol{y}}_u$ contains all, and only, the information dependent entries of $\bar{\boldsymbol{y}}_u$.

Proof: When TH is absent, $c_u^{\mathrm{th}}(k) = 0$, $\forall k$, implies that $\boldsymbol{\Theta} = \boldsymbol{I}_{N_fN_p}$ and $\boldsymbol{\Psi} = \boldsymbol{0}$ in (14). The resulting $\bar{\boldsymbol{y}}_u$ becomes $(\mathcal{E}_u/N_f)^{1/2} s_u\ (\boldsymbol{c}_u \otimes \bar{\boldsymbol{\alpha}}) + \bar{\boldsymbol{\eta}}$. Using properties of Kronecker products, we have $(\boldsymbol{I}_{N_f} \otimes \boldsymbol{S})^{\mathrm{T}}(\boldsymbol{c}_u \otimes \bar{\boldsymbol{\alpha}}) = \boldsymbol{c}_u \otimes (\boldsymbol{S}^{\mathrm{T}} \bar{\boldsymbol{\alpha}}) = \boldsymbol{c}_u \otimes \tilde{\boldsymbol{\alpha}}$. It then readily follows that $\boldsymbol{y}_u = (\mathcal{E}_u/N_f)^{1/2} s_u\ (\boldsymbol{c}_u \otimes \tilde{\boldsymbol{\alpha}}) + (\boldsymbol{I}_{N_f} \otimes \boldsymbol{S})^{\mathrm{T}} \bar{\boldsymbol{\eta}}$. This is identical to (9), where all, and only, the information dependent terms are present. ■

Removing excess entries from $\bar{\boldsymbol{y}}_u$ is much more complicated when TH is also present. To this end, we establish the following:

Lemma 2: For any Rake selection matrix $\boldsymbol{S}$, we can extract the information-bearing entries from $\bar{\boldsymbol{y}}_u$ by forming $\boldsymbol{y}_u = \boldsymbol{\Xi}_0^{\mathrm{T}} \bar{\boldsymbol{y}}_u$, where $\boldsymbol{\Xi}_0 := [\,\boldsymbol{\Xi}_A \quad \boldsymbol{\Xi}_B\,]$, and

$$\boldsymbol{\Xi}_A := \boldsymbol{\Theta}\left(\boldsymbol{I}_{N_f} \otimes \boldsymbol{S}\right) \mathrm{diag}\left\{\boldsymbol{T}_{N,M_0}, \ldots, \boldsymbol{T}_{N,M_{N_f-1}}\right\}$$

$$\boldsymbol{\Xi}_B := \boldsymbol{\Psi}\left(\boldsymbol{I}_{N_f} \otimes \boldsymbol{S}\right) \mathrm{diag}\left\{\boldsymbol{\Upsilon}_{N,\bar{M}_0}, \ldots, \boldsymbol{\Upsilon}_{N,\bar{M}_{N_f-1}}\right\} \quad (15)$$

with $M_k := \sum_{n=0}^{\bar{c}_u^{\mathrm{th}}(k)-1} [\boldsymbol{S} \cdot \boldsymbol{1}_{N\times 1}]_n$, $\bar{M}_k := N - M_k$, $\forall k \in [0, N_f - 1]$, and $\boldsymbol{\Upsilon}_{N,M_k} := [\boldsymbol{0}_{M_k,N-M_k}\ \boldsymbol{I}_{M_k}]^{\mathrm{T}}$ being a zero-prefix matrix that attaches $(N - M_k)$ zeros at the beginning of an $M_k \times 1$ vector.

Proof: See Appendix I. ■

Premultiplying $\bar{\boldsymbol{y}}_u$ with $\boldsymbol{\Xi}_0 = [\,\boldsymbol{\Xi}_A \quad \boldsymbol{\Xi}_B\,]$ retains all, and only, the information dependent entries and gives rise to

$$\boldsymbol{y}_u = \sqrt{\frac{\mathcal{E}_u}{N_f}} s_u \left(\begin{bmatrix} \boldsymbol{\Xi}_A^{\mathrm{T}}\boldsymbol{\Theta} \\ \boldsymbol{\Xi}_B^{\mathrm{T}}\boldsymbol{\Psi} \end{bmatrix} (\boldsymbol{c}_u \otimes \bar{\boldsymbol{\alpha}}) + \begin{bmatrix} \boldsymbol{\Xi}_A^{\mathrm{T}}\boldsymbol{\Psi} \\ \boldsymbol{\Xi}_B^{\mathrm{T}}\boldsymbol{\Theta} \end{bmatrix} (\boldsymbol{c}_u \otimes \bar{\boldsymbol{\alpha}}) \right) + \boldsymbol{\Xi}_0^{\mathrm{T}} \bar{\boldsymbol{\eta}}. \quad (16)$$

In the absence of TH, $\boldsymbol{\Xi}_0$ simplifies to $(\boldsymbol{I}_{N_f} \otimes \boldsymbol{S})$, and $\boldsymbol{y}_u$ coincides with that in Lemma 1. But when TH is present, entries of $\boldsymbol{y}_u$ in (16) are *not* guaranteed to be distinct. To see this, let us take a closer look at the IFI term that is captured by the second summand in (16). As detailed in Appendix II, both $\boldsymbol{\Xi}_A^{\mathrm{T}}\boldsymbol{\Psi}(\boldsymbol{c}_u \otimes \bar{\boldsymbol{\alpha}})$ and $\boldsymbol{\Xi}_B^{\mathrm{T}}\boldsymbol{\Theta}(\boldsymbol{c}_u \otimes \bar{\boldsymbol{\alpha}})$ have a block structure with the kth block given by

$$c_u(k-1)\boldsymbol{T}_{N,M_k}^{\mathrm{T}} \boldsymbol{S}^{\mathrm{T}} \left(\boldsymbol{J}_{N_p}^{\mathrm{T}}\right)^{c_u^{\mathrm{th}}(k)+\bar{c}_u^{\mathrm{th}}(k-1)} \bar{\boldsymbol{\alpha}}$$

$$c_u(k+1)\boldsymbol{\Upsilon}_{N,\bar{M}_k}^{\mathrm{T}} \boldsymbol{S}^{\mathrm{T}} \left(\boldsymbol{J}_{N_p}\right)^{c_u^{\mathrm{th}}(k+1)+\bar{c}_u^{\mathrm{th}}(k)} \bar{\boldsymbol{\alpha}} \quad (17)$$

respectively. Evidently, they depend not only on the relative difference of two successive TH codes: $c_u^{\mathrm{th}}(k) + \bar{c}_u^{\mathrm{th}}(k-1) = N_p + c_u^{\mathrm{th}}(k) - c_u^{\mathrm{th}}(k-1)$, but also on the delay selection matrix $\boldsymbol{S}$. These IFI terms vanish $\forall \boldsymbol{S}$ if and only if $c_u^{\mathrm{th}}(k) \geq c_u^{\mathrm{th}}(k-1)$; that is, when $c_u^{\mathrm{th}}(k) = 0$, $\forall k$. The presence of TH can lead to overlapping of Rake delays corresponding to adjacent pulses, which in turn may give rise to IFI. Each so-induced IFI term involves two correlator output samples from two consecutive pulses. To form $\boldsymbol{y}_u$, every pair of these interfering samples in $\bar{\boldsymbol{y}}_u$ is picked up twice: once during the earlier frame duration captured by $\boldsymbol{\Xi}_A$; and a second time during the later frame captured by $\boldsymbol{\Xi}_B$. As a result, the matrix $\boldsymbol{\Xi}_0 = [\,\boldsymbol{\Xi}_A \quad \boldsymbol{\Xi}_B\,]$ is not guaranteed to be full column rank, and entries of $\boldsymbol{y}_u$ in (16) are thus *not* guaranteed to be distinct.

Having clarified the source of repetitions in $\boldsymbol{y}_u$ in (16), we deduce that repetitions can be eliminated by removing redundant entries in $\boldsymbol{\Xi}_B^{\mathrm{T}}\boldsymbol{\Theta}(\boldsymbol{c}_u \otimes \bar{\boldsymbol{\alpha}})$ while keeping $\boldsymbol{\Xi}_A^{\mathrm{T}}\boldsymbol{\Psi}(\boldsymbol{c}_u \otimes \bar{\boldsymbol{\alpha}})$ untouched, or vice versa. Without loss of generality, we choose the former, and establish the following:

Lemma 3: For any Rake selection matrix $\boldsymbol{S}$, $\boldsymbol{\Xi} = [\,\boldsymbol{\Xi}_A \quad \boldsymbol{\Xi}_C\,]$ is full column rank with $\boldsymbol{\Xi}_C$ given as

$$\boldsymbol{\Xi}_C = \boldsymbol{\Xi}_B\,[\,\boldsymbol{e}_{n_1} \quad \ldots \quad \boldsymbol{e}_{n_K}\,], \quad K = \mathrm{rank}\{\boldsymbol{\Xi}_0\} - \sum_{n=0}^{N_f-1} M_k$$

where $\boldsymbol{e}_n$ is the nth column of the identity matrix $\boldsymbol{I}_{\bar{M}}$ with $\bar{M} := \sum_{n=0}^{N_f-1} \bar{M}_k$, and $\{n_k\}_{k=1}^K$ are indices of the zero entries of the $\bar{M} \times 1$ vector $\boldsymbol{v} := \boldsymbol{\Xi}_B^{\mathrm{T}}\boldsymbol{\Xi}_A \boldsymbol{1}_{(N_fN-\bar{M})\times 1}$. Then the resulting vector that contains all (and only those) nonzero correlator outputs, without repetition, is given by

$$\boldsymbol{y}_u = \sqrt{\frac{\mathcal{E}_u}{N_f}} s_u \boldsymbol{\Xi}^{\mathrm{T}}(\boldsymbol{\Theta} + \boldsymbol{\Psi})(\boldsymbol{c}_u \otimes \bar{\boldsymbol{\alpha}}) + \boldsymbol{\eta} \quad (18)$$

where $\boldsymbol{\eta} := \boldsymbol{\Xi}^{\mathrm{T}} \bar{\boldsymbol{\eta}}$.

Proof: See Appendix III. ■

It can be easily verified that the length of $\boldsymbol{y}_u$ in (18) is $\sum_{n=0}^{N_f-1} M_k + K = \mathrm{rank}\{\boldsymbol{\Xi}_0\} \leq N_fN$, where the equality is achieved if and only if $\boldsymbol{\Xi}_0$ is full rank, in which case, $\boldsymbol{\Xi} = \boldsymbol{\Xi}_0$.

The MF and MMSE weights corresponding to (18) are, respectively: $\boldsymbol{\beta}_{\mathrm{mf}} = \boldsymbol{\Xi}^{\mathrm{T}}(\boldsymbol{\Theta} + \boldsymbol{\Psi})(\boldsymbol{c}_u \otimes \bar{\boldsymbol{\alpha}})$; and $\boldsymbol{\beta}_{\mathrm{mmse}} = (\mathcal{E}_u/N_f)\boldsymbol{R}_\eta^{-1}\boldsymbol{\Xi}^{\mathrm{T}}(\boldsymbol{\Theta} + \boldsymbol{\Psi})(\boldsymbol{c}_u \otimes \bar{\boldsymbol{\alpha}})[1 + (\mathcal{E}_u/N_f)(\boldsymbol{c}_u \otimes \bar{\boldsymbol{\alpha}})^{\mathrm{T}}(\boldsymbol{\Theta} + \boldsymbol{\Psi})^{\mathrm{T}}\boldsymbol{\Xi}\boldsymbol{R}_\eta^{-1}\boldsymbol{\Xi}^{\mathrm{T}}(\boldsymbol{\Theta} + \boldsymbol{\Psi})(\boldsymbol{c}_u \otimes \bar{\boldsymbol{\alpha}})]^{-1}$.

Remark 1: Equations (9) and (18) are our unifying digital models for general Rake reception. Established based on a two-step (correlation followed by weighted combination) approach, (9) and (18) require frame-rate sampling per finger. Interestingly, receiver processing can be implemented even with symbol-rate sampling. To prove this, recall first that the entries of $\boldsymbol{\beta}$ (that is, $[\boldsymbol{\beta}]_n \forall n$) are the diversity combining weights. In the absence of TH, Rake reception that yields the decision statistics z_u can be realized by correlating $r_u(t)$ with the *symbol-long* template $\bar{p}_s(t) = \sum_{k=0}^{N_f-1} \sum_{n=0}^{N-1} [\boldsymbol{\beta}]_{kN+n}\ p(t - kT_f - \tilde{\tau}_n)$, and sampling its output every $T_s = N_fT_f$ seconds. In the presence of TH, the *symbol-long* template becomes $\bar{p}_s(t) = \sum_{k=0}^{N_f-1} \sum_{n=0}^{M_k+K_k-1} [\boldsymbol{\beta}]_{\theta(k,n)}\, p(t - kT_f - c_u^{\mathrm{th}}(k)T_c - \tilde{\tau}_n)$,

where $\theta(k,n) := \sum_{m=0}^{k-1} M_m + n$, if $n < M_k$, and $\theta(k,n) := \sum_{m\neq k} M_m + \sum_{m=0}^{k-1} K_m + n$, if $n \geq M_k$. It can also be verified that, with or without TH, MF combining can be implemented using the template $\bar{p}_f(t) := \sum_{n=0}^{N_f-1} \tilde{\alpha}_n p(t-\tilde{\tau}_n)$, which has fixed combining weights that do not change across frames. The decision statistic is thus given by $z_u = \sum_{k=0}^{N_f-1} c_u(k) \int r_u(t) \bar{p}_f(t - kT_f - c_u^{\rm th}(k)T_c) {\rm d}t$. In other words, Rake reception with $\boldsymbol{\beta}_{\rm mf}$ can be carried out frame by frame; whereas with $\boldsymbol{\beta}_{\rm mmse}$, Rake can only be performed on a symbol-by-symbol basis. This also indicates that NBI renders frame-by-frame receiver processing suboptimal.

To generate the template $\bar{p}_s(t)$, multiple analog waveforms $p(t)$ have to be generated and delayed accordingly. The delay accuracy will affect decoding performance. But different from pulse-rate sampling that requires precise timing at each sampling instance, $\bar{p}_s(t)$ needs to be generated only once during the channel coherence time. The latter provides the timing circuits sufficient time to stabilize and thus reduces timing jitter effects.

Remark 2: Carried out for binary PAM, our analysis and I/O models in (9) and (18) hold for binary pulse-position modulation (PPM) as well. For binary PPM, one only needs to replace the correlator template $p(t)$ with $p(t) - p(t-\Delta)$, where Δ is the PPM modulation index.

IV. SINR Analysis

In this section, we will compare performance of different transmission schemes based on their corresponding SINRs for different selections of $\boldsymbol{\beta}$. To carry out these SINR-based comparisons, we will rely on our general I/O relationship (9) for the TH-free case, and its counterpart (18) when TH is present.

In the *absence* of TH, the instantaneous SINR after diversity combining for the two receiver options is given by [cf. (9)]

$$\text{SINR}_{\rm mf} := \frac{N_f \mathcal{E}_u |\tilde{\boldsymbol{\alpha}}^{\rm T} \tilde{\boldsymbol{\alpha}}|^2}{(\boldsymbol{c}_u \otimes \tilde{\boldsymbol{\alpha}})^{\rm T} \boldsymbol{R}_\eta (\boldsymbol{c}_u \otimes \tilde{\boldsymbol{\alpha}})} \tag{19}$$

and

$$\text{SINR}_{\rm mmse} := \frac{\mathcal{E}_u}{N_f} (\boldsymbol{c}_u \otimes \tilde{\boldsymbol{\alpha}})^{\rm T} \boldsymbol{R}_\eta^{-1} (\boldsymbol{c}_u \otimes \tilde{\boldsymbol{\alpha}}) \tag{20}$$

respectively, where $\boldsymbol{R}_\eta = (\boldsymbol{I}_{N_f} \otimes \boldsymbol{S}^{\rm T}) \boldsymbol{R}_{\bar{\eta}} (\boldsymbol{I}_{N_f} \otimes \boldsymbol{S})$. Recall that with $\bar{\boldsymbol{\eta}}$ being stationary Gaussian, its correlation matrix $\boldsymbol{R}_{\bar{\eta}}$ is an $N_f N_p \times N_f N_p$ Toeplitz matrix. Since $N_f N_p$ is large ($\gg$100), $\boldsymbol{R}_{\bar{\eta}}$ can be well approximated by a circulant matrix, which can be diagonalized by FFT matrices as in [14]; i.e., $\boldsymbol{F}_{N_f N_p} \boldsymbol{R}_{\bar{\eta}} \boldsymbol{F}_{N_f N_p}^{\mathcal{H}} \approx \boldsymbol{\Phi}$, where $\boldsymbol{\Phi}$ is a diagonal matrix. In particular, if the NBI has a flat power spectral density on its nonzero frequency support, the nth diagonal entry of the diagonal matrix $\boldsymbol{\Phi}$ is given by

$$[\boldsymbol{\Phi}]_{n,n} = \begin{cases} \dfrac{J_0 + N_0}{2}, & \text{if subband } n \text{ is hit} \\ \dfrac{N_0}{2}, & \text{otherwise} \end{cases}, \quad n \in [0, N_f N_c) \tag{21}$$

where $N_0/2$ is the AWGN power and $J_0/2$ is the NBI power. Fig. 2(c) depicts an example of $\boldsymbol{F}_{N_f N_p} \boldsymbol{R}_{\bar{\eta}} \boldsymbol{F}_{N_f N_p}^{\mathcal{H}}$. The interferer has a flat PSD with power $J_0/N_0 = 8$ dB and $N_0/2 = 1$. Notice that with $N_f N_p = 4 \times 16 = 64$, $\boldsymbol{F}_{N_f N_p} \boldsymbol{R}_{\bar{\eta}} \boldsymbol{F}_{N_f N_p}^{\mathcal{H}}$ is approximately diagonal, as indicated in (21).

So far, we have developed closed-form expressions for the SINR at the Rake outputs based on our unifying digital model (9). It follows from (19) and (20) that SINR is generally code dependent, which in turn implies that the BER generally depends on $\boldsymbol{c}_u$. However, it is possible to have code-independent SINR. For example, we know that when $\boldsymbol{\eta}$ is white, the MMSE weights boil down to MF weights and for all transmission schemes we have from (19) that: $\text{SINR}_{\rm mmse} = \text{SINR}_{\rm mf} = (2\mathcal{E}_u/N_0) \tilde{\boldsymbol{\alpha}}^{\rm T} \tilde{\boldsymbol{\alpha}}$, since $(\boldsymbol{c}_u \otimes \tilde{\boldsymbol{\alpha}})^{\rm T} (\boldsymbol{c}_u \otimes \tilde{\boldsymbol{\alpha}}) = \boldsymbol{c}_u^{\rm T} \boldsymbol{c}_u \tilde{\boldsymbol{\alpha}}^{\rm T} \tilde{\boldsymbol{\alpha}} = N_f \tilde{\boldsymbol{\alpha}}^{\rm T} \tilde{\boldsymbol{\alpha}}$. In *narrowband* systems, it has also been shown that the performance of MC-CDMA is code independent [14]. One may expect a similar result to hold for our real baseband MC-UWB with Rake reception. In fact, we will prove that the BER of real MC-UWB systems is indeed code independent, with any Rake finger selection, even in the presence of NBI and dense multipath, as we summarize in the following proposition.

Proposition 1: In baseband MC-UWB with codes $c_u(k) = \boldsymbol{g}_k^{\rm T} \boldsymbol{c}_u^{(o)}$, $\forall u$, $k \in [0, N_f - 1]$, where no TH is employed, the SINR in (19) and (20) corresponding to MF and MMSE Rake receivers are code/user independent even in the presence of NBI, regardless of the multipath channel and the Rake finger delay selection, as long as $\{|\bar{c}_u^{(o)}(k)|^2\}_{k=0}^{N_f-1}$ are the same $\forall u \in [0, N_f - 1]$.

Proof: See Appendix IV. ■

Code-independent SINR implies that the corresponding BER is also code independent. As an example, consider $\boldsymbol{c}_u^{(o)}$ in (5) with binary $\{\pm 1\}$ entries. In this case, $|\bar{c}_u^{(o)}(k)|^2 = 1$, $\forall k$, $u \in [0, N_f - 1]$. The BER corresponding to such $\boldsymbol{c}_u^{(o)}$ will thus be code independent.

Unique to MC-UWB, Proposition 1 can also be justified intuitively. Recall that each MC-UWB user utilizes all N_f digital subcarriers, with each MC subcarrier occupying distinct frequency bands. When $\{|\bar{c}_u^{(o)}(k)|^2$ for each k is constant across all users $u \in [0, N_f - 1]$, all users have the same 'weight' on each subcarrier and its corresponding frequency bands. Therefore, NBI affects all users (codes) uniformly. In particular, when $|\bar{c}_u^{(o)}(k)|^2 = 1$, $\forall k$, $u \in [0, N_f - 1]$, each user's transmit PSD will be 'flat' (see also Fig. 1).

In the *presence* of TH, the instantaneous SINR after diversity combining for the two receiver options is given, respectively, by [cf. (18)]

$$\text{SINR}_{\rm mf} = \frac{N_f \mathcal{E}_u \left| (\boldsymbol{c}_u \otimes \bar{\boldsymbol{\alpha}})^{\rm T} (\boldsymbol{\Theta} + \boldsymbol{\Psi})^{\rm T} \boldsymbol{\Xi} \boldsymbol{\Xi}^{\rm T} (\boldsymbol{\Theta} + \boldsymbol{\Psi}) (\boldsymbol{c}_u \otimes \bar{\boldsymbol{\alpha}}) \right|^2}{(\boldsymbol{c}_u \otimes \bar{\boldsymbol{\alpha}})^{\rm T} (\boldsymbol{\Theta} + \boldsymbol{\Psi})^{\rm T} \boldsymbol{\Xi} \boldsymbol{R}_\eta \boldsymbol{\Xi}^{\rm T} (\boldsymbol{\Theta} + \boldsymbol{\Psi}) (\boldsymbol{c}_u \otimes \bar{\boldsymbol{\alpha}})} \tag{22}$$

and

$$\text{SINR}_{\rm mmse} := \frac{\mathcal{E}_u}{N_f} (\boldsymbol{c}_u \otimes \bar{\boldsymbol{\alpha}})^{\rm T} (\boldsymbol{\Theta} + \boldsymbol{\Psi})^{\rm T} \boldsymbol{\Xi} \boldsymbol{R}_\eta^{-1} \boldsymbol{\Xi}^{\rm T} (\boldsymbol{\Theta} + \boldsymbol{\Psi}) (\boldsymbol{c}_u \otimes \bar{\boldsymbol{\alpha}}) \tag{23}$$

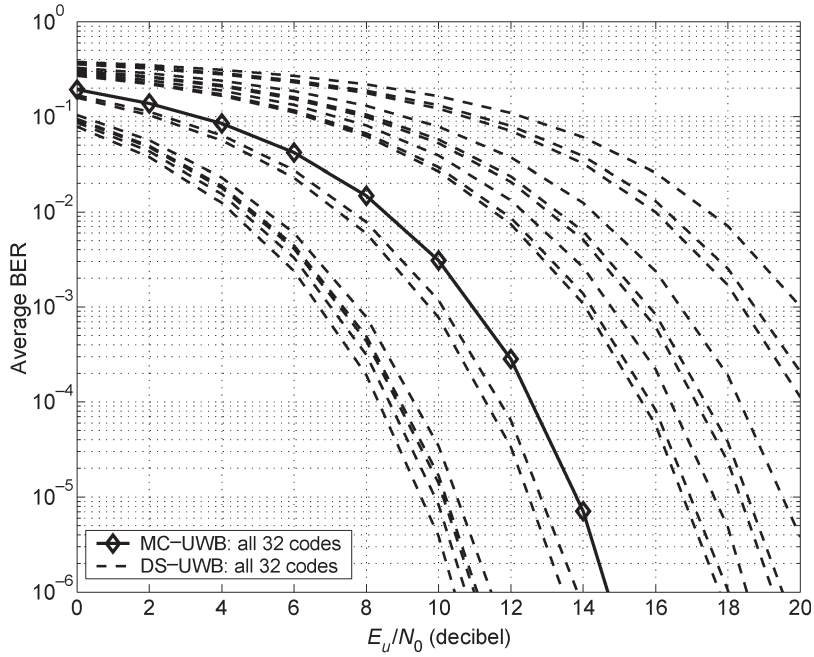

Fig. 3. BER for DS- and MC-UWB over AWGN channels with NBI-1 (center frequency 1.2 GHz, bandwidth 20 MHz). MMSE-Rake with $N = 1$ is used. The performance of all codes is plotted to illustrate code (in)dependence.

where $\boldsymbol{R}_\eta = \boldsymbol{\Xi}^{\mathrm{T}} \boldsymbol{R}_{\bar{\eta}} \boldsymbol{\Xi}$. In the absence of IFI, we have $\boldsymbol{\Xi}_C = \boldsymbol{\Xi}_B$. Vanishing $\boldsymbol{\Xi}_A \boldsymbol{\Psi}$ and $\boldsymbol{\Xi}_B \boldsymbol{\Theta}$ reduces the noise-free part of (16) to

$$\boldsymbol{\Xi}^{\mathrm{T}}(\boldsymbol{\Theta}+\boldsymbol{\Psi})(\boldsymbol{c}_u \otimes \bar{\boldsymbol{\alpha}}) = \sqrt{\frac{\mathcal{E}_u}{N_f}} s_u(n_s) \begin{bmatrix} \boldsymbol{\Xi}_A^{\mathrm{T}} \boldsymbol{\Theta}(\boldsymbol{c}_u \otimes \bar{\boldsymbol{\alpha}}) \\ \boldsymbol{\Xi}_B^{\mathrm{T}} \boldsymbol{\Psi}(\boldsymbol{c}_u \otimes \bar{\boldsymbol{\alpha}}) \end{bmatrix}$$

which is nothing but the noise-free part of (9) premultiplied by an $N_f N \times N_f N$ permutation matrix [cf. (26) and (27)]. As a result, (22) and (23) boil down to (19) and (20).

V. Simulations and Numerical Results

In our simulations, the number of frames per symbol is chosen as $N_f = 32$. A Gaussian monocycle with duration $T_p = 0.7$ ns is used as the pulse shaper $p(t)$. Since the UWB transmission here is baseband real, the multipath channels are generated using the S–V channel model [8] modified as in [4], where channel taps are real. The parameters to generate random channel realizations are chosen as $(1/\Lambda, 1/\lambda, \Gamma, \gamma) = (43, 0.4, 7.1, 4.3)$ ns, giving rise to maximum excess delays around 35 ns. We truncate the channel taps at $\tau_L = 34$ ns and choose $T_f = 35$ ns. As a result, we obtain $N_p := T_f/T_p = 50$. The TH codes are generated independently from a uniform distribution over $[0, N_c - 1]$. Two N_c values are used: $N_c = 10$ with $T_c = 3.5$ ns, and $N_c = 50$ with $T_c = 0.7$ ns. We use Walsh–Hadamard (W–H) codes for DS-UWB and as the orthogonal codes $\boldsymbol{c}_u^{(o)}$ for the MC-UWB spreading in (5). In our simulations, selective- and partial-Rake are employed, where the N delays with strongest outputs are chosen for the former, and the first N delays are chosen for the latter. In AWGN channels, we use $N = 1$. When multipath is also present, more fingers are used and will be specified in individual simulations. These results are generated using (19), (20), (22), and (23), averaged over 5000 channel realizations each associated with a random TH code.

Three sets of parameters are used to generate NBI with a flat inband power spectrum: NBI-1 with 1.2-GHz center frequency and 20-MHz bandwidth; NBI-2 with 900-MHz center frequency and 25-MHz bandwidth; and NBI-3 with 900-MHz center frequency and 80-MHz bandwidth. Notice that NBI-1 approximates the GPS band and NBI-2 approximates the GSM900 band. The power of NBI is $J_0/N_0 = 30$ dB relative to the AWGN power N_0.

In Figs. 3 and 4, we plot BER corresponding to all 32 DS and MC spreading codes, in AWGN channels with a 1-finger MMSE-Rake receiver, and in multipath channels with a 16-finger selective MF-Rake receiver, both in the presence of NBI. Corroborating Proposition 1, MC exhibits identical performance across all codes/users; whereas DS exhibits code-dependent performance, in both AWGN and multipath channels with NBI. But as it is clear from Figs. 5 and 6, which depict BER over multipath channels with MMSE-Rake, performance variation among different DS codes decreases as the number of Rake fingers increases from 1 to 16. Also notice that though selective-Rake improves performance of all codes, it also increases the performance variation across codes, in comparison to partial-Rake reception.

When random TH is also present, the performance corresponding to all DS and MC spreading codes is shown in Fig. 7 for AWGN channels. Unlike the TH-absent case, MC codes exhibit more pronounced performance variation than DS codes. This suggests that the code-independence property of MC spreading is very sensitive to TH.

When NBI is present but multipath is absent, the BER average over all DS, SC, and MC spreading codes is depicted in Fig. 8 in the presence of NBI-1 (GPS) interferer. We observe

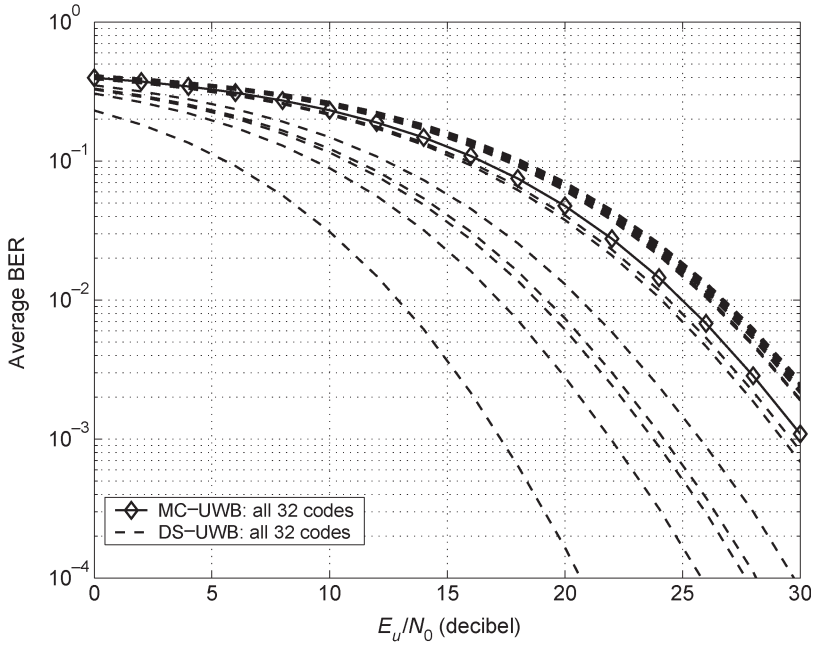

Fig. 4. BER for DS- and MC-UWB over multipath channels with NBI-1 (center frequency 1.2 GHz, bandwidth 20 MHz). Selective-Rake with MF combining and $N = 16$ is used. The performance of all codes is plotted to illustrate code (in)dependence.

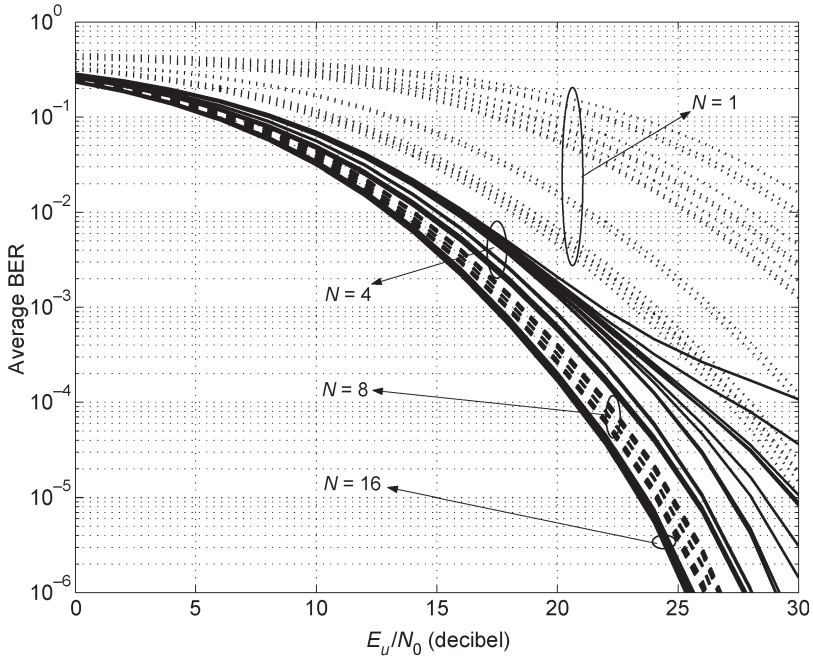

Fig. 5. BER for DS-UWB over multipath channels with NBI-1 (center frequency 1.2 GHz, bandwidth 20 MHz). Selective-Rake with MMSE combining and various number of fingers: $N = 1, 4, 8, 16$. The performance of all codes is plotted to illustrate code dependence.

that DS- and SC-UWB yield a similar performance, while MC-UWB outperforms both. In Fig. 9, we also plot the average BER of DS-, SC-, and MC-UWB in the presence of three different jammers. These jammers have the same bandwidth but different center frequencies. As shown in the figure, MC-UWB yields invariant performance, while DS- and SC-UWB exhibit variable BER, as the jammer's center frequency changes.

In the presence of both NBI and multipath effects, the average BER *versus* $\mathcal{E}_u/N_0$ is depicted in Fig. 10 for DS/SC/MC-UWB. Notice that MC-UWB outperforms others, whereas the performance difference diminishes as more Rake fingers are employed. To compare selective- and partial-Rake, we also plot in Fig. 11 the average BER of MC-UWB with $N = 4$, 8, 16 Rake fingers. As expected, MMSE-Rake outperforms MF-Rake, and selective-Rake yields a universally better performance than partial-Rake. But the improvement is more evident for smaller values of N.

With TH codes also being employed, we plot in Fig. 12 the average BER for DS/SC/MC–TH, and TH-only UWB, over AWGN channels with $N = 1$ and $N_c = 10$. Comparing Fig. 12

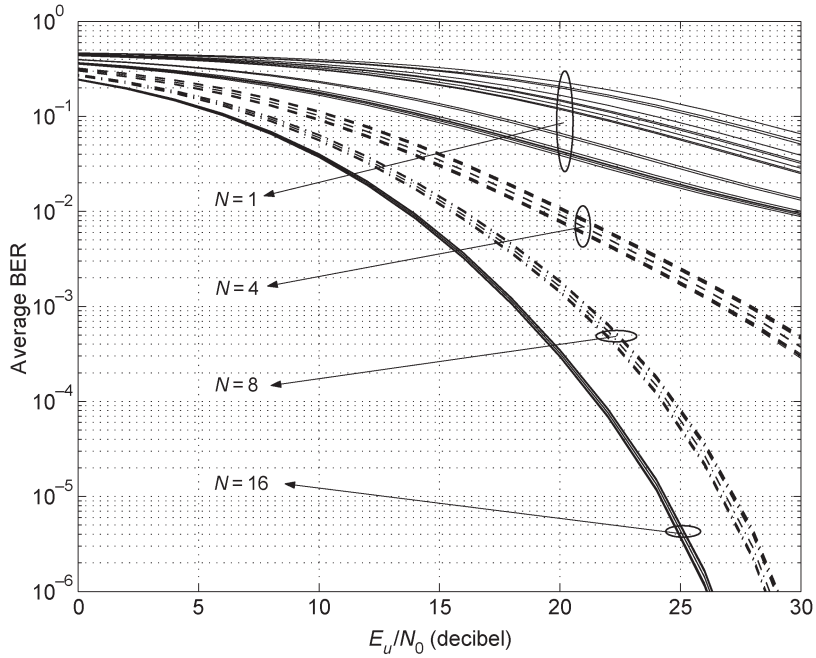

Fig. 6. BER for DS-UWB over multipath channels with NBI-1 (center frequency 1.2 GHz, bandwidth 20 MHz). Partial-Rake with MMSE combining and various number of fingers: $N = 1, 4, 8, 16$. The performance of all codes is plotted to illustrate code dependence.

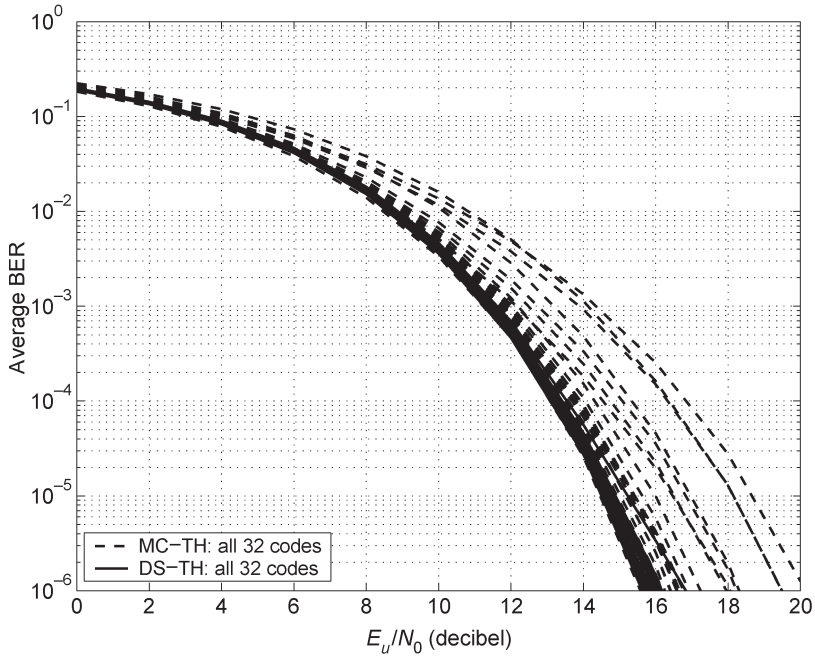

Fig. 7. BER for DS–TH- and MC–TH-UWB over AWGN channels with NBI-1 (center frequency 1.2 GHz, bandwidth 20 MHz). MMSE-Rake with $N = 1$ is used. The performance of all codes is plotted to illustrate code dependence.

with Fig. 8, we observe that in AWGN channels, TH improves performance of DS and SC, but adversely affects MC. In the presence of multipath, we plot the average BER for DS/SC/MC-UWB with and without TH in Fig. 13, in the presence of NBI-3. TH consistently improves the performance of all DS/SC/MC codes, with $N_c = 50$ and various number of Rake fingers $N = 1, 4, 8, 16$. But the improvement is not as significant as in AWGN channels, and no difference among spreading codes is observed.

VI. Conclusion

In this paper, we developed a unifying transmission and Rake reception model for UWB radios, which encompasses several spreading codes including not only the well known DS and TH codes, but also the recent SC and MC codes, and their combinations. Our unifying model accounts for the IFI induced by TH and multipath channels and allows for various Rake finger delay selections. Moreover, without invoking oversampling, this model is established in digital form, which enables

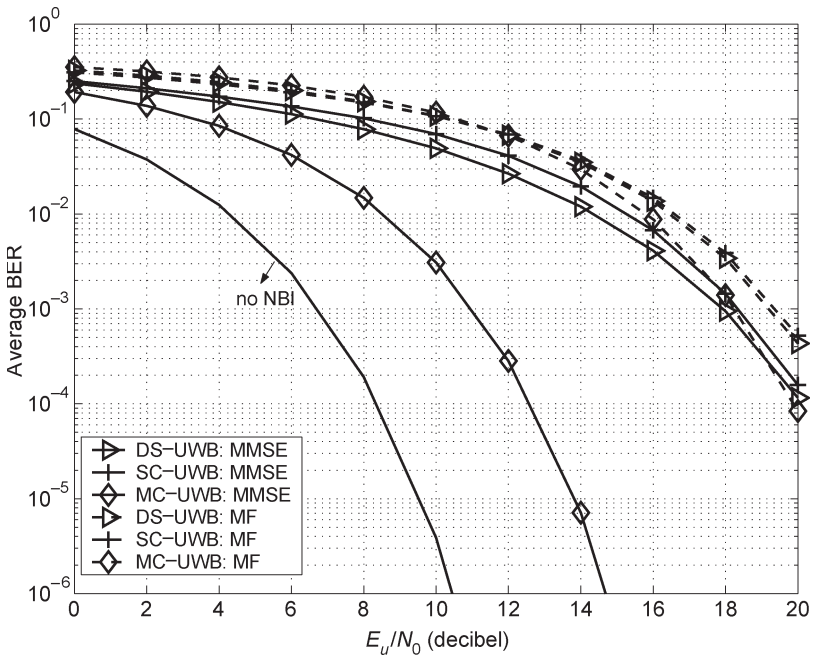

Fig. 8. Average BER corresponding to DS-, SC-, and MC-UWB over AWGN with NBI-1 (center frequency 1.2 GHz, bandwidth 20 MHz).

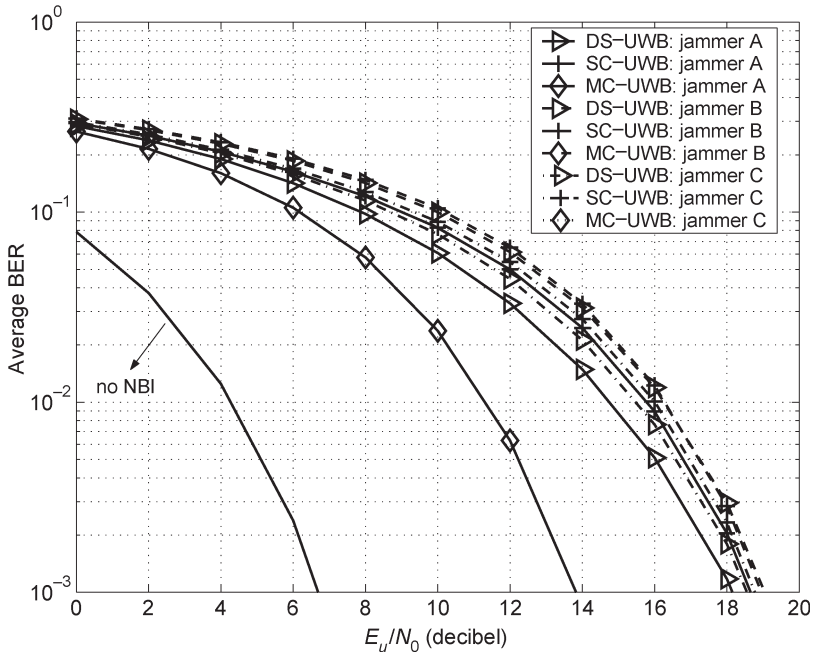

Fig. 9. Average BER corresponding to DS-, SC-, and MC-UWB over AWGN channels, in the presence of three 25-MHz bandwidth jammers with different center frequencies: Jammer A (300 MHz), Jammer B (400 MHz), and Jammer C (900 MHz).

closed-form SINR expressions. Based on these expressions, we studied and compared the effects of NBI in both AWGN and dense multipath channels, for various types of UWB transmissions.

Our simulation results corroborate the code-independent BER performance of MC-UWB in the presence of multipath and NBI effects, regardless of the Rake finger selection. We also observed that with MMSE combining, both partial- and selective-Rake receivers are able to reduce the performance variation across individual codes, as the number of Rake fingers increases. Moreover, while selective-Rake results in a better BER performance than partial-Rake, the former induces a larger variation across individual codes. Finally, TH improves performance of all DS/SC/MC codes in multipath channels. But in AWGN channels, although MC spreading codes yield superior performance than DS and SC codes in the absence of TH, the presence of TH seems to be more favorable to DS and SC codes.

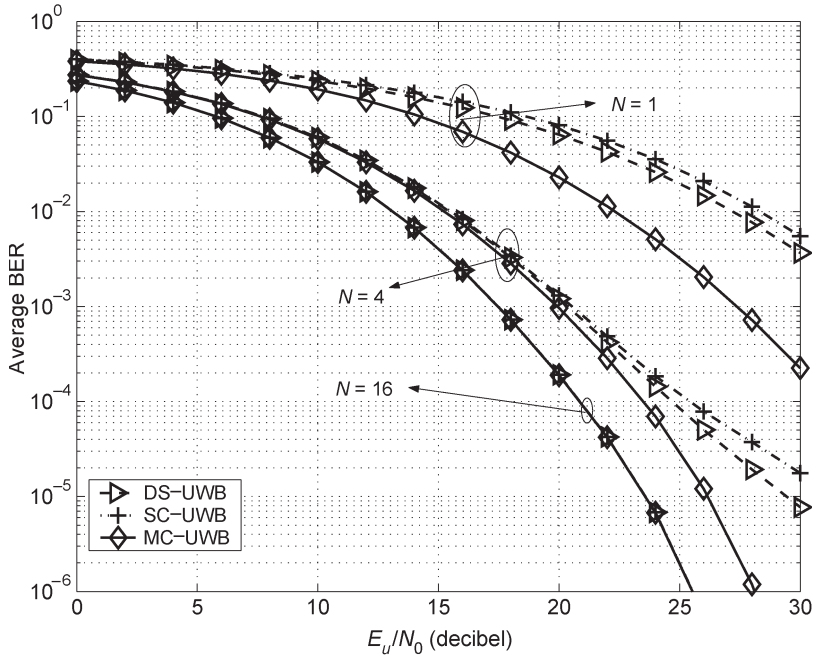

Fig. 10. Average BER corresponding to DS-, SC-, and MC-UWB over dense multipath channels with AWGN, in the presence of NBI-1 (center frequency 1.2 GHz, bandwidth 20 MHz). Selective-Rake with $N = 1, 4, 16$ fingers is used.

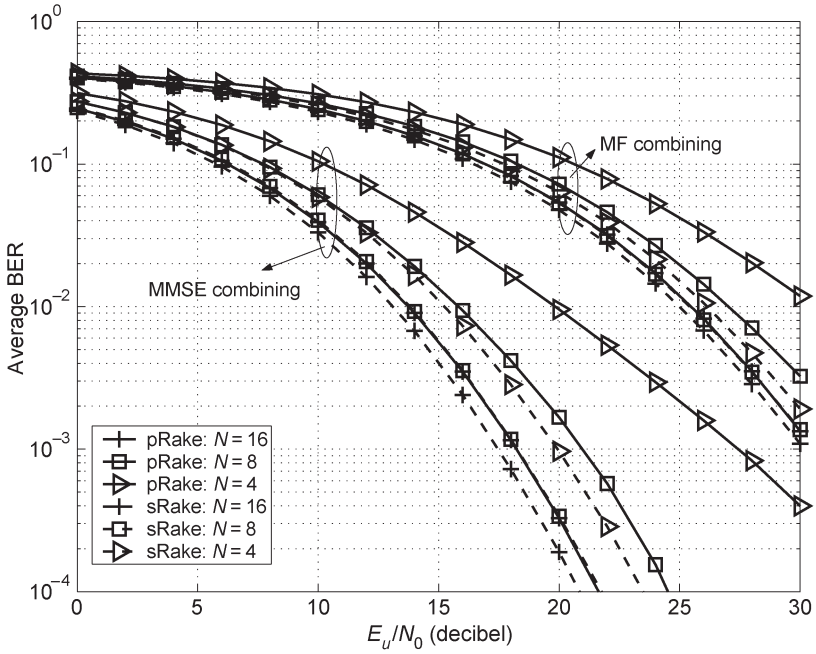

Fig. 11. Average BER of MC-UWB over multipath channels with AWGN, in the presence of NBI-1: partial-Rake (pRake) *versus* selective-Rake (sRake) with various N values.

APPENDIX I
PROOF OF LEMMA 2

After processing $\bar{\boldsymbol{y}}_u$ with $\boldsymbol{\Xi}_0 = [\,\boldsymbol{\Xi}_A \quad \boldsymbol{\Xi}_B\,]$, the resultant vector $\boldsymbol{y}_u = \boldsymbol{\Xi}_0^{\mathrm{T}} \bar{\boldsymbol{y}}_u$ is given by

$$\boldsymbol{y}_u = \sqrt{\frac{\mathcal{E}_u}{N_f}} s_u \left(\left[\boldsymbol{\Xi}_A^{\mathrm{T}} \boldsymbol{\Theta} \boldsymbol{\Xi}_B^{\mathrm{T}} \boldsymbol{\Psi} \right] (\boldsymbol{c}_u \otimes \bar{\boldsymbol{\alpha}}) + \left[\boldsymbol{\Xi}_A^{\mathrm{T}} \boldsymbol{\Psi} \boldsymbol{\Xi}_B^{\mathrm{T}} \boldsymbol{\Theta} \right] (\boldsymbol{c}_u \otimes \bar{\boldsymbol{\alpha}}) \right) + \boldsymbol{\Xi}^{\mathrm{T}} \bar{\boldsymbol{\eta}}. \quad (24)$$

To specify the entries of this vector, let us start with its component $\boldsymbol{\Xi}_A^{\mathrm{T}} \boldsymbol{\Theta} (\boldsymbol{c}_u \otimes \bar{\boldsymbol{\alpha}})$. Recall that matrices $\boldsymbol{\Xi}_A$ and $\boldsymbol{\Theta}$ as well as vector $\boldsymbol{c}_u \otimes \bar{\boldsymbol{\alpha}}$ all have block structures. Consequently, $\boldsymbol{\Xi}_A^{\mathrm{T}} \boldsymbol{\Theta} (\boldsymbol{c}_u \otimes \bar{\boldsymbol{\alpha}})$ is also a block-structured vector, whose kth block is

$$c_u(k) \boldsymbol{T}_{N,M_k}^{\mathrm{T}} \boldsymbol{S}^{\mathrm{T}} \boldsymbol{A}_k^{\mathrm{T}} \boldsymbol{A}_k \bar{\boldsymbol{\alpha}} = c_u(k) \boldsymbol{T}_{N,M_k}^{\mathrm{T}} \tilde{\boldsymbol{\alpha}} \quad (25)$$

where $M_k := \sum_{n=0}^{\bar{c}_u^{\mathrm{th}}(k)-1} [\boldsymbol{S} \cdot \boldsymbol{1}_{N\times 1}]_n$. Intuitively, M_k is nothing but the number of Rake correlations on the kth pulse

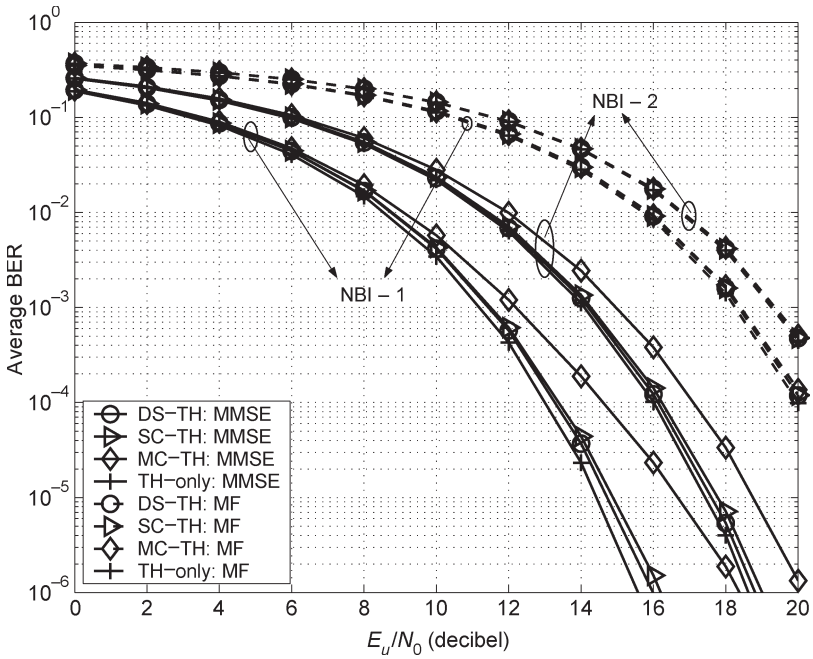

Fig. 12. Average BER corresponding to DS/SC/MC–TH and TH-only UWB over AWGN channels, in the presence of NBI-1 (center frequency 1.2 GHz, bandwidth 20 MHz) and NBI-2 (center frequency 900 MHz, bandwidth 25 MHz).

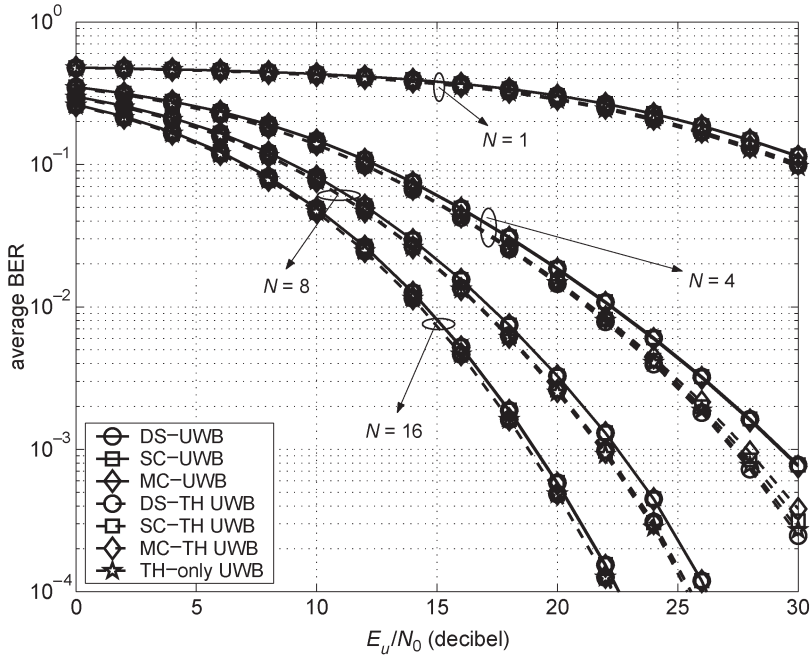

Fig. 13. Average BER corresponding to DS/SC/MC-UWB with and without TH, over multipath channels with AWGN, in the presence of NBI-3 (center frequency 900 MHz, bandwidth 80 MHz). Partial-Rake receiver with $N = 1, 4, 8, 16$ fingers and MMSE combining.

within the "current" (kth) frame duration. In the absence of TH, one would have $M_k = N$, $\forall k$. But when TH is present, the delays $\{c_u^{\rm th}(k)T_c + \tilde{\tau}_n\}_{n=0}^{N-1}$ corresponding to the kth pulse are not guaranteed to fall into the kth frame duration, due to the TH-induced shift $c_u^{\rm th}(k)T_c$. In other words, some of the Rake delays will spill over to the next frame duration. Evidently, the number of Rake delays that fall into the "next" [$(k+1)$th] frame duration is $\bar{M}_k = N - M_k$. With (25), it readily follows that

$$\boldsymbol{\Xi}_A^{\rm T}\boldsymbol{\Theta}(\boldsymbol{c}_u \otimes \bar{\boldsymbol{\alpha}}) = \left[\, c_u(0)\tilde{\boldsymbol{\alpha}}^{\rm T}\boldsymbol{T}_{N,M_0} \quad \cdots \quad c_u(N_f-1)\tilde{\boldsymbol{\alpha}}^{\rm T}\boldsymbol{T}_{N,M_{N_f-1}} \,\right]^{\rm T}. \tag{26}$$

For each (say, the kth) frame duration, the vector $c_u(k)\boldsymbol{T}_{N,M_k}^{\mathrm{T}}\tilde{\boldsymbol{\alpha}}$ collects M_k correlator outputs corresponding to the "current" (the kth) pulse. Concatenation of these vectors across frames then yields the $(\sum_{k=0}^{N_f-1} M_k)\times 1$ vector in (26).

As to the component $\boldsymbol{\Xi}_B^{\mathrm{T}}\boldsymbol{\Psi}(\boldsymbol{c}_u\otimes\bar{\boldsymbol{\alpha}})$, it can be readily verified that $\boldsymbol{\Psi}^{\mathrm{T}}\boldsymbol{\Psi}=\mathrm{diag}\{\boldsymbol{B}_0^{\mathrm{T}}\boldsymbol{B}_0,\ldots,\boldsymbol{B}_{N_f-2}^{\mathrm{T}}\boldsymbol{B}_{N_f-2},\boldsymbol{0}_{N_c\times N_c}\}$. Consequently, the kth block of this component has a form similar to (25), and is given by: $c_u(k)\boldsymbol{\Upsilon}_{N,\bar{M}_k}^{\mathrm{T}}\boldsymbol{S}^{\mathrm{T}}\boldsymbol{B}_k^{\mathrm{T}}\boldsymbol{B}_k\bar{\boldsymbol{\alpha}}=c_u(k)\boldsymbol{\Upsilon}_{N,\bar{M}_k}^{\mathrm{T}}\tilde{\boldsymbol{\alpha}}$. As a result, we obtain the following vector:

$$\boldsymbol{\Xi}_B^{\mathrm{T}}\boldsymbol{\Psi}(\boldsymbol{c}_u\otimes\bar{\boldsymbol{\alpha}}) = \left[\begin{array}{ccc} c_u(0)\tilde{\boldsymbol{\alpha}}^{\mathrm{T}}\boldsymbol{\Upsilon}_{N,\bar{M}_0}^{\mathrm{T}} & \ldots & c_u(N_f-2)\tilde{\boldsymbol{\alpha}}^{\mathrm{T}}\boldsymbol{\Upsilon}_{N,\bar{M}_{N_f-2}}\end{array}\right]^{\mathrm{T}} \tag{27}$$

which has $\sum_{k=0}^{N_f-2}\bar{M}_k$ elements. Interestingly, vectors in (26) and (27) do not share common elements, simply because $\boldsymbol{\Upsilon}_{N,\bar{M}_k}^{\mathrm{T}}\boldsymbol{T}_{N,M_k}=\boldsymbol{0}_{\bar{M}_k\times M_k}$ by definition.

Stacking (26) and (27), we deduce that the first term in (24) contains N_fN distinct correlator outputs, which are dependent on $\tilde{\boldsymbol{\alpha}}$. This confirms that all noise-only entries of $\bar{\boldsymbol{y}}_u$ are removed when premultiplied with $\boldsymbol{\Xi}_0^{\mathrm{T}}=[\,\boldsymbol{\Xi}_A\quad\boldsymbol{\Xi}_B\,]^{\mathrm{T}}$.

To show that all entries being removed are noise-only ones, notice that the maximum number of correlator outputs is N_fN; that is, N correlator outputs per pulse and N_f pulses per symbol. The size of $\boldsymbol{y}_u$ indicates that no correlator output is removed from $\bar{\boldsymbol{y}}_u$.

APPENDIX II
PROOF OF (17)

To specify structures of $\boldsymbol{\Xi}_A^{\mathrm{T}}\boldsymbol{\Psi}(\boldsymbol{c}_u\otimes\bar{\boldsymbol{\alpha}})$ and $\boldsymbol{\Xi}_B^{\mathrm{T}}\boldsymbol{\Theta}(\boldsymbol{c}_u\otimes\bar{\boldsymbol{\alpha}})$, first notice that $\boldsymbol{\Theta}^{\mathrm{T}}\boldsymbol{\Psi}=\mathrm{diag}\{\boldsymbol{0}_{N_c\times N_c},\boldsymbol{A}_1^{\mathrm{T}}\boldsymbol{B}_0,\ldots,\boldsymbol{A}_{N_f-1}^{\mathrm{T}}\boldsymbol{B}_{N_f-2}\}\ (\boldsymbol{J}_{N_f}\otimes\boldsymbol{I}_{N_c})$. Their kth blocks can then be shown to be, respectively

$$c_u^{\mathrm{th}}(k-1)\boldsymbol{T}_{N,M_k}^{\mathrm{T}}\boldsymbol{S}^{\mathrm{T}}\boldsymbol{A}_k^{\mathrm{T}}\boldsymbol{B}_{k-1}\bar{\boldsymbol{\alpha}}$$
$$c_u^{\mathrm{th}}(k+1)\boldsymbol{\Upsilon}_{N,\bar{M}_k}^{\mathrm{T}}\boldsymbol{S}^{\mathrm{T}}\boldsymbol{B}_k^{\mathrm{T}}\boldsymbol{A}_{k+1}\bar{\boldsymbol{\alpha}}$$

where matrices $\boldsymbol{A}$ and $\boldsymbol{B}$ have different indices due to the shift matrix $\boldsymbol{J}_{N_f}$. Using definitions of matrices $\boldsymbol{A}$ and $\boldsymbol{B}$, we deduce that the kth block of $\boldsymbol{\Xi}_A^{\mathrm{T}}\boldsymbol{\Psi}(\boldsymbol{c}_u\otimes\bar{\boldsymbol{\alpha}})$ is $c_u(k-1)\boldsymbol{T}_{N,M_k}^{\mathrm{T}}\boldsymbol{S}^{\mathrm{T}}(\boldsymbol{J}_{N_c}^{\mathrm{T}})^{c_u^{\mathrm{th}}(k)+\bar{c}_u^{\mathrm{th}}(k-1)}\bar{\boldsymbol{\alpha}}$, and that of $\boldsymbol{\Xi}_B^{\mathrm{T}}\boldsymbol{\Theta}(\boldsymbol{c}_u\otimes\bar{\boldsymbol{\alpha}})$ is $c_u(k+1)\boldsymbol{\Upsilon}_{N,\bar{M}_k}^{\mathrm{T}}\boldsymbol{S}^{\mathrm{T}}(\boldsymbol{J}_{N_c})^{c_u^{\mathrm{th}}(k+1)+\bar{c}_u^{\mathrm{th}}(k)}\bar{\boldsymbol{\alpha}}$.

APPENDIX III
PROOF OF LEMMA 3

For any Rake selection matrix $\boldsymbol{S}$, premultiplying $\bar{\boldsymbol{y}}_u$ with $\boldsymbol{\Xi}_0^{\mathrm{T}}=[\,\boldsymbol{\Xi}_A\quad\boldsymbol{\Xi}_B\,]^{\mathrm{T}}$ eliminates all the noise-only entries of $\bar{\boldsymbol{y}}_u$. To further remove possible repetitions in $\boldsymbol{\Xi}_0^{\mathrm{T}}\bar{\boldsymbol{y}}_u$, one needs to first find the locations of these redundant entries. Next, we will argue that these locations are indicated by nonzero entries in the matrix-product $\boldsymbol{\Xi}_B^{\mathrm{T}}\boldsymbol{\Xi}_A$.

As $\boldsymbol{\Xi}_0$ is not guaranteed to be full rank, it may contain pairs of identical columns, for the reasons stated before Lemma 3. For the same reasons, each pair of these identical columns must be included separately in $\boldsymbol{\Xi}_B$ and $\boldsymbol{\Xi}_A$. As a result, nonzero entries of the cross product $\boldsymbol{\Xi}_B^{\mathrm{T}}\boldsymbol{\Xi}_A$ indicate the existence of redundant entries and their locations (indices) in $\boldsymbol{y}_u=\boldsymbol{\Xi}_0^{\mathrm{T}}\bar{\boldsymbol{y}}_u$. More specifically, the column index of a nonzero entry of $\boldsymbol{\Xi}_B^{\mathrm{T}}\boldsymbol{\Xi}_A$ indicates the corresponding $\bar{\boldsymbol{y}}_u$ entry's first appearance in $\boldsymbol{y}_u$, which is captured by $\boldsymbol{\Xi}_A$; and the row index of it indicates the same $\bar{\boldsymbol{y}}_u$ entry's second appearance in $\boldsymbol{y}_u$, which is captured by $\boldsymbol{\Xi}_B$.

In order to remove one of the two appearances/repetitions, one only needs to capture the column (or equivalently, row) index of its corresponding nonzero entry in $\boldsymbol{\Xi}_B^{\mathrm{T}}\boldsymbol{\Xi}_A$. To this end, we simply postmultiply $\boldsymbol{\Xi}_B^{\mathrm{T}}\boldsymbol{\Xi}_A$ with an all-one vector to form vector $\boldsymbol{v}:=\boldsymbol{\Xi}_B^{\mathrm{T}}\boldsymbol{\Xi}_A\cdot\boldsymbol{1}_{(N_fN-\bar{M})\times 1}$. The nonzero entries of the latter turn out to be all ones, whose indices indicate the second appearances of redundant entries in $\boldsymbol{\Xi}_B^{\mathrm{T}}\bar{\boldsymbol{y}}_u$. With the size of the latter being N_fN, it readily follows that the number of redundant entries is $(N_fN-\mathrm{rank}\{\boldsymbol{\Xi}_0\})$, which is identical to the number of nonzero entries in the vector $\boldsymbol{v}$.

As a result, keeping only those columns of $\boldsymbol{\Xi}_B$ which correspond to zero entries of $\boldsymbol{v}$ guarantees elimination of all (and only) redundant entries of $\boldsymbol{\Xi}_0^{\mathrm{T}}\bar{\boldsymbol{y}}_u$. Therefore, for any Rake selection matrix $\boldsymbol{S}$, choosing $\boldsymbol{\Xi}=[\,\boldsymbol{\Xi}_A\quad\boldsymbol{\Xi}_C\,]$ with $\boldsymbol{\Xi}_C$ as in Lemma 3 enables extraction of all, and only, information dependent entries from $\bar{\boldsymbol{y}}_u$, without any repetition.

APPENDIX IV
PROOF OF PROPOSITION 1

Using properties of Kronecker products, we have: $\boldsymbol{c}_u\otimes\tilde{\boldsymbol{\alpha}}=(\boldsymbol{c}_u\otimes\boldsymbol{I}_N)\tilde{\boldsymbol{\alpha}}$. Moreover, (5) can be expressed as: $\boldsymbol{c}_u=\boldsymbol{F}_{N_f}^{\mathcal{H}}\bar{\boldsymbol{c}}_u^{(o)}$, where $\{\bar{\boldsymbol{c}}_u^{(o)}\}_{u=0}^{N_f-1}$ are new code vectors constructed from $\boldsymbol{c}_u^{(o)}$:

$$\left[\bar{\boldsymbol{c}}_u^{(o)}\right]_k = \begin{cases} \left[\boldsymbol{c}_u^{(o)}\right]_k, & \text{if } k=0, \text{or } \frac{N_f}{2} \\ \frac{1}{\sqrt{2}}\left(\left[\boldsymbol{c}_u^{(o)}\right]_k+\jmath\cdot\left[\boldsymbol{c}_u^{(o)}\right]_{N_f-k}\right), & \text{if } k\in\left[1,\frac{N_f}{2}\right) \\ \frac{1}{\sqrt{2}}\left(\left[\boldsymbol{c}_u^{(o)}\right]_{N_f-k}-\jmath\cdot\left[\boldsymbol{c}_u^{(o)}\right]_k\right), & \text{if } k\in\left[\frac{N_f}{2}+1,N_f\right) \end{cases}.$$

It turns out that: i) if the original vectors $\boldsymbol{c}_u^{(o)}$ are orthogonal, then $\bar{\boldsymbol{c}}_u^{(o)}$ are also orthogonal, i.e., $(\bar{\boldsymbol{c}}_{u_1}^{(o)})^{\mathcal{H}}\bar{\boldsymbol{c}}_{u_2}^{(o)}=N_f\delta_{u_1u_2}$; and ii) if entries of $\boldsymbol{c}_u^{(o)}$ take binary $\{\pm1\}$ values, then entries of $\bar{\boldsymbol{c}}_u^{(o)}$ are complex numbers on the unit circle. Using $\bar{\boldsymbol{c}}_u^{(o)}$, an alternative expression of $\boldsymbol{c}_u\otimes\tilde{\boldsymbol{\alpha}}$ can be obtained

$$\boldsymbol{c}_u\otimes\tilde{\boldsymbol{\alpha}}=\left(\boldsymbol{F}_{N_f}^{\mathcal{H}}\bar{\boldsymbol{c}}_u^{(o)}\otimes\boldsymbol{I}_N\right)\tilde{\boldsymbol{\alpha}}=\left(\boldsymbol{F}_{N_f}\otimes\boldsymbol{I}_N\right)^{\mathcal{H}}\left(\bar{\boldsymbol{c}}_u^{(o)}\otimes\boldsymbol{I}_N\right)\tilde{\boldsymbol{\alpha}}.$$

Consider now the denominator of $\mathrm{SINR}_{\mathrm{mf}}$ in (19). Replacing $(\boldsymbol{c}_u\otimes\tilde{\boldsymbol{\alpha}})$ with its alternative expression, the denominator becomes

$$(\boldsymbol{c}_u\otimes\tilde{\boldsymbol{\alpha}})^{\mathrm{T}}\boldsymbol{R}_\eta(\boldsymbol{c}_u\otimes\tilde{\boldsymbol{\alpha}})=\tilde{\boldsymbol{\alpha}}^{\mathrm{T}}\left(\bar{\boldsymbol{c}}_u^{(o)}\otimes\boldsymbol{I}_N\right)^{\mathcal{H}}\bar{\boldsymbol{R}}\left(\bar{\boldsymbol{c}}_u^{(o)}\otimes\boldsymbol{I}_N\right)\tilde{\boldsymbol{\alpha}}$$

with $\bar{\boldsymbol{R}} := (\boldsymbol{F}_{N_f} \otimes \boldsymbol{I}_N)\boldsymbol{R}_\eta(\boldsymbol{F}_{N_f} \otimes \boldsymbol{I}_N)^{\mathcal{H}}$. Using the definition of $\boldsymbol{R}_\eta$, properties of Kronecker product and the approximation $\boldsymbol{R}_{\bar{\eta}} \approx \boldsymbol{F}^{\mathcal{H}}_{N_pN_f}\boldsymbol{\Phi}\boldsymbol{F}_{N_pN_f}$, we deduce that

$$\bar{\boldsymbol{R}} := \left(\boldsymbol{F}_{N_f} \otimes \boldsymbol{S}^{\mathrm{T}}\right)\boldsymbol{F}^{\mathcal{H}}_{N_pN_f}\boldsymbol{\Phi}\boldsymbol{F}_{N_pN_f}\left(\boldsymbol{F}^{\mathcal{H}}_{N_f} \otimes \boldsymbol{S}\right).$$

It can be readily verified that the $(m+1, n+1)$th element of the product $(\boldsymbol{F}_{N_f} \otimes \boldsymbol{S}^{\mathrm{T}})\boldsymbol{F}^{\mathcal{H}}_{N_pN_f}$ is

$$\frac{1}{\sqrt{N_p}}\mathrm{e}^{\jmath\frac{2\pi}{N_pN_f}i \bmod (m,N)\left\lfloor\frac{m}{N}\right\rfloor}\mathrm{e}^{\jmath\frac{2\pi}{N_p}i \bmod (m,N)\left\lfloor\frac{n}{N_f}\right\rfloor}\delta_{n,\left\lfloor\frac{n}{N_f}\right\rfloor N_f+\left\lfloor\frac{m}{N}\right\rfloor}$$

$\forall m \in [0, NN_f-1]$, and $n \in [0, N_pN_f-1]$. Casting into a matrix form, we have $(\boldsymbol{F}_{N_f} \otimes \boldsymbol{S}^{\mathrm{T}})\boldsymbol{F}^{\mathcal{H}}_{N_pN_f} = \boldsymbol{D}(\boldsymbol{I}_{N_f} \otimes \boldsymbol{F}_{N_p}\boldsymbol{S})^{\mathcal{H}}\boldsymbol{P}$, where $\boldsymbol{P}$ is an $N_cN_f \times N_pN_f$ permutation matrix whose $(n+1)$th column is $\boldsymbol{e}_{\lfloor n/N_f\rfloor+N_p\cdot \bmod (n,N_f)+1}$, and $\boldsymbol{D} := (\boldsymbol{I}_{N_f} \otimes \boldsymbol{S}^{\mathrm{T}})\bar{\boldsymbol{D}}(\boldsymbol{I}_{N_f} \otimes \boldsymbol{S})$ with diagonal matrix $\bar{\boldsymbol{D}}$ having entries $[\bar{\boldsymbol{D}}]_{n,n} = \exp[\jmath(2\pi/N_pN_f)\cdot\lfloor n/N_p\rfloor\cdot \bmod(n,N_p)]$, $\forall n \in [0, N_pN_f-1]$. As a result, the product $\bar{\boldsymbol{R}}$ becomes

$$\bar{\boldsymbol{R}} = \boldsymbol{D}\left(\boldsymbol{I}_{N_f} \otimes \boldsymbol{F}_{N_p}\boldsymbol{S}\right)^{\mathcal{H}}\boldsymbol{P}\boldsymbol{\Phi}\boldsymbol{P}^{\mathrm{T}}\left(\boldsymbol{I}_{N_f} \otimes \boldsymbol{F}_{N_p}\boldsymbol{S}\right)\boldsymbol{D}^{\mathcal{H}}.$$

With $\boldsymbol{\Phi}$ being a diagonal matrix, $\bar{\boldsymbol{\Phi}} := \boldsymbol{P}\boldsymbol{\Phi}\boldsymbol{P}^{\mathrm{T}}$ is also a diagonal matrix, because $\boldsymbol{P}$ is a permutation matrix. The $(n+1)$th diagonal entry of $\bar{\boldsymbol{\Phi}}$ turns out to be $[\bar{\boldsymbol{\Phi}}]_{n,n} = [\boldsymbol{\Phi}]_{\lfloor n/N_f\rfloor+N_p\cdot \bmod (n,N_f)}$. Moreover, notice that $\boldsymbol{D}$ is a diagonal matrix, and $(\boldsymbol{I}_{N_f} \otimes \boldsymbol{F}^{\mathcal{H}}_N)$ is a block-diagonal matrix. Consequently, their product $\bar{\boldsymbol{R}}$ must also be a block-diagonal matrix consisting of N_f submatrices on its diagonal, each of size $N \times N$.

Denoting the $(k+1)$th submatrix of the block-diagonal matrix $\bar{\boldsymbol{R}}$ as $\bar{\boldsymbol{R}}_k$, $\forall k \in [0, N_f-1]$, the denominator of $\mathrm{SINR}_{\mathrm{mf}}$ in (19) becomes

$$\begin{aligned}
&(\boldsymbol{c}_u \otimes \tilde{\boldsymbol{\alpha}})^{\mathrm{T}}\boldsymbol{R}_\eta(\boldsymbol{c}_u \otimes \tilde{\boldsymbol{\alpha}}) \\
&\quad= \tilde{\boldsymbol{\alpha}}^{\mathrm{T}}\left(\bar{\boldsymbol{c}}^{(o)}_u \otimes \boldsymbol{I}_N\right)^{\mathcal{H}}\mathrm{diag}\left\{\bar{\boldsymbol{R}}_1, \ldots, \bar{\boldsymbol{R}}_{N_f-1}\right\}\left(\bar{\boldsymbol{c}}^{(o)}_u \otimes \boldsymbol{I}_N\right)\tilde{\boldsymbol{\alpha}} \\
&\quad= \tilde{\boldsymbol{\alpha}}^{\mathrm{T}}\sum_{k=0}^{N_f-1}\bar{c}^{(o)*}_u(k)\bar{\boldsymbol{R}}_k\bar{c}^{(o)}_u(k)\tilde{\boldsymbol{\alpha}} \\
&\quad= \sum_{k=0}^{N_f-1}\left|\bar{c}^{(o)}_u(k)\right|^2\cdot(\tilde{\boldsymbol{\alpha}}^{\mathrm{T}}\bar{\boldsymbol{R}}_k\tilde{\boldsymbol{\alpha}}).
\end{aligned}$$

Evidently, as long as $\{|\bar{c}^{(o)}_u(k)|^2\}_{k=0}^{N_f-1}$ do not depend on u, the SINR corresponding to MF combining will be independent of spreading codes.

Similarly, consider the $\mathrm{SINR}_{\mathrm{mmse}}$ in (20) for MMSE combining. From the fact that $(\boldsymbol{c}_u \otimes \tilde{\boldsymbol{\alpha}})^{\mathrm{T}}\boldsymbol{R}^{-1}_\eta(\boldsymbol{c}_u \otimes \tilde{\boldsymbol{\alpha}}) = \tilde{\boldsymbol{\alpha}}^{\mathrm{T}}(\bar{\boldsymbol{c}}^{(o)}_u \otimes \boldsymbol{I}_N)^{\mathcal{H}}\bar{\boldsymbol{R}}^{-1}(\bar{\boldsymbol{c}}^{(o)}_u \otimes \boldsymbol{I}_N)\tilde{\boldsymbol{\alpha}}$, we deduce that

$$\mathrm{SINR}_{\mathrm{mmse}} = \frac{\mathcal{E}_u}{N_f}\sum_{k=0}^{N_f-1}\left|\bar{c}^{(o)}_u(k)\right|^2\cdot\left(\tilde{\boldsymbol{\alpha}}^{\mathrm{T}}\bar{\boldsymbol{R}}^{-1}_k\tilde{\boldsymbol{\alpha}}\right).$$

Once again, we observe that the SINR is code independent, so long as $\{|\bar{c}^{(o)}_u(k)|^2\}_{k=0}^{N_f-1}$ do not change across users $u \in [0, N_f-1]$.

REFERENCES

[1] I. Bergel, E. Fishler, and H. Messer, "Narrow-band interference suppression in time-hopping impulse-radio systems," in *Proc. Conf. Ultra Wideband Systems and Technologies*, Baltimore, MD, 2002, pp. 303–307.

[2] D. Cassioli, M. Z. Win, F. Vatalaro, and A. F. Molisch, "Performance of low-complexity Rake reception in a realistic UWB channel," in *Proc. Int. Conf. Communications*, New York, 2002, pp. 763–767.

[3] G. Durisi, A. Tarable, J. Romme, and S. Benedetto, "A general method for error probability computation of UWB systems for indoor multiuser communications," *J. Commun. Netw.*, vol. 5, no. 4, pp. 354–364, Dec. 2003.

[4] J. Foerster, *Channel Modeling Sub-Committee Report Final*, Nov. 2002. IEEE P802.15-02/368r5-SG3a, IEEE P802.15 Working Group for WPAN.

[5] J. R. Foerster, "The performance of a direct-sequence spread ultra wideband system in the presence of multipath, narrowband interference, and multiuser interference," in *Proc. Conf. Ultra Wideband Systems and Technologies*, Baltimore, MD, 2002, pp. 87–92.

[6] M. Hämäläinen, V. Hovinen, R. Tesi, J. Iinatti, and M. Latva-aho, "On the UWB system coexistence with GSM900, umts/wcdma, and GPS," *IEEE J. Sel. Areas Commun.*, vol. 20, no. 9, pp. 1712–1721, Dec. 2002.

[7] B. M. Sadler and A. Swami, "On the performance of UWB and DS-spread spectrum communication systems," in *Proc. Conf. Ultra Wideband Systems and Technologies*, Baltimore, MD, 2002, pp. 289–292.

[8] A. A. M. Saleh and R. A. Valenzuela, "A statistical model for indoor multipath propagation," *IEEE J. Sel. Areas Commun.*, vol. SAC-5, no. 2, pp. 128–137, Feb. 1987.

[9] R. A. Scholtz, "Multiple access with time-hopping impulse modulation," in *Proc. Military Communications (MILCOM) Conf.*, Boston, MA, 1993, pp. 447–450.

[10] M. Z. Win and R. A. Scholtz, "On the energy capture of ultrawide bandwidth signals in dense multipath environments," *IEEE Commun. Lett.*, vol. 2, no. 9, pp. 245–247, Sep. 1998.

[11] L. Yang and G. B. Giannakis, "Multi-stage block-spreading for impulse radio multiple access through ISI channels," *IEEE J. Sel. Areas Commun.*, vol. 20, no. 9, pp. 1767–1777, Dec. 2002.

[12] ——, "Digital-carrier multi-band user codes for baseband UWB multiple access," *J. Commun. Netw.*, vol. 5, no. 4, pp. 374–385, Dec. 2003.

[13] L. Zhao and A. M. Haimovich, "Performance of ultra-wideband communications in the presence of interference," *IEEE J. Sel. Areas Commun.*, vol. 20, no. 9, pp. 1684–1691, Dec. 2002.

[14] S. Zhou, G. B. Giannakis, and A. Swami, "Digital multi-carrier spread-spectrum versus direct-sequence spread-spectrum for resistance to jamming and multipath," *IEEE Trans. Commun.*, vol. 50, no. 4, pp. 643–655, Apr. 2002.

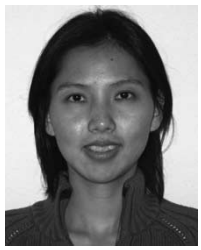

Liuqing Yang (S'02–M'04) received the B.S. degree in electrical engineering from the Huazhong University of Science and Technology, Wuhan, China, in 1994, and the M.Sc. and Ph.D. degrees in electrical and computer engineering from the University of Minnesota, Minneapolis, in 2002 and 2004, respectively.

Since August 2004, she has been an Assistant Professor at the Department of Electrical and Computer Engineering, University of Florida, Gainesville. Her research interests include communications, signal processing, and networking. Currently, she has particular interest in ultra-wideband (UWB) communications. Her research encompasses synchronization, channel estimation, equalization, multiple access, space-time coding, and multicarrier systems.

Georgios B. Giannakis (S'84–M'86–SM'91–F'97) received the Diploma in electrical engineering from the National Technical University of Athens, Greece, in 1981, and the M.Sc. degree in electrical engineering, the M.Sc. degree in mathematics, and the Ph.D. degree in electrical engineering from the University of Southern California (USC), Los Angeles, in 1983, 1986, and 1986, respectively.

After lecturing for 1 year at USC, he joined the University of Virginia, Charlottesville, in 1987, where he became a Professor of Electrical Engineering in 1997. Since 1999, he has been a Professor at the Department of Electrical and Computer Engineering, University of Minnesota, Minneapolis, where he now holds an ADC Chair in Wireless Telecommunications. His general interests span the areas of communications and signal processing, estimation and detection theory, time-series analysis, and system identification—subjects on which he has published more than 220 journal papers, 380 conference papers, and two edited books. Current research focuses on transmitter and receiver diversity techniques for single- and multiuser fading communication channels, complex-field and space-time coding, multi-carrier ultrawide band wireless communication systems, cross-layer designs, and sensor networks.

Dr. Giannakis is the (co)recipient of six paper awards from the IEEE Signal Processing (SP) and Communications Societies (1992, 1998, 2000, 2001, 2003, and 2004). He also received the IEEE-Signal Processing Society's Technical Achievement Award in 2000 and European Association for Signal, Speech and Image Processing (EURASIP) Technical Achievement Award in 2005. He served as Editor-in-Chief for the IEEE SIGNAL PROCESSING LETTERS, as Associate Editor for the IEEE TRANSACTIONS ON SIGNAL PROCESSING and the IEEE SIGNAL PROCESSING LETTERS, as Secretary of the Signal Processing Conference Board, as Member of the Signal Processing Publications Board, as Member and Vice-Chair of the Statistical Signal and Array Processing Technical Committee, as Chair of the Signal Processing for Communications Technical Committee, and as a Member of the IEEE Fellows Election Committee. He has also served as a Member of the IEEE-Signal Processing Society's Board of Governors, the Editorial Board for the PROCEEDINGS OF THE IEEE, and the Steering Committee of the IEEE TRANSACTIONS ON WIRELESS COMMUNICATIONS.